

GALAXY LUMINOSITY FUNCTIONS TO $Z \sim 1$: DEEP2 VS. COMBO-17 AND IMPLICATIONS FOR RED GALAXY FORMATION¹

S. M. FABER², C. N. A. WILLMER^{2,3}, C. WOLF⁴, D. C. KOO², B. J. WEINER⁵, J. A. NEWMAN^{6,7}, M. IM⁸, A. L. COIL⁹, C. CONROY⁹, M. C. COOPER⁹, M. DAVIS⁹, D. P. FINKBEINER¹⁰, B. F. GERKE⁹, K. GEBHARDT^{7,12}, E. J. GROTH¹³, P. GUHATHAKURTA², J. HARKER², N. KAISER¹⁴, S. KASSIN², M. KLEINHEINRICH¹⁵, N. P. KONIDARIS², L. LIN^{2,16}, G. LUPPINO¹⁴, D. S. MADGWICK^{6,7,8}, K. MEISENHEIMER¹⁵, K. G. NOESKE², A. C. PHILLIPS², V. L. SARAJEDINI¹⁷, L. SIMARD¹⁸, A. S. SZALAY¹⁹, N. P. VOGT²⁰, R. YAN⁸

Draft version February 2, 2008

ABSTRACT

The DEEP2 and COMBO-17 surveys are used to study the evolution of the luminosity function of red and blue galaxies to $z \sim 1$. Schechter function fits show that, since $z = 1$, M_B^* dims by ~ 1.3 mag per unit redshift for both color classes, ϕ^* of blue galaxies shows little change, while ϕ^* for red galaxies has formally nearly quadrupled. At face value, the number density of blue galaxies has remained roughly constant since $z = 1$, whereas that of red galaxies has been rising. Luminosity densities support both conclusions, but we note that most red-galaxy evolution occurs between our data and local surveys and in our highest redshift bin, where the data are weakest. We discuss the implications of having most red galaxies emerge after $z = 1$ from precursors among the blue population, taking into account the properties of local and distant E/S0s. We suggest a “mixed” scenario in which some blue galaxies have their star-formation quenched in gas-rich mergers, migrate to the red sequence with a variety of masses, and merge further on the red sequence in one or more purely stellar mergers. E/S0s of a given mass today will have formed via different routes, in a manner that may help to explain the fundamental plane and other local scaling laws.

Subject headings: Galaxies: distances and redshifts – galaxies: luminosity function – galaxies: evolution

1. INTRODUCTION

A major handicap in lookback studies of galaxy evolution is the inability to follow the evolution of any one galaxy over time. Instead, we see only snapshots of the galaxy population at different epochs, and it is difficult to identify objects at one epoch with their precursors and descendants at different epochs. One of the most important tools to solve this problem is precision counts of galaxies, which can quantify the “flow” of galaxies in parameter space as masses, morphologies, and stellar populations change. The luminosity function of galaxies was historically the first such tool, but the concept is rapidly being broadened to include counts as a function of mass, internal velocity, color, and other parameters.

A further difficulty is caused by the fact that nearly all

functions known to date are *unimodal* and lack clear features that demarcate one class of galaxies from another. In other words, galaxies tend to populate one big “cloud” in most parameter spaces rather than separate clumps. This makes interpretation difficult, as sub-counts depend on how boundaries within these clouds are defined, and it is not clear whether (or how) these boundaries should be adjusted to follow galaxy evolution. As a result, we often cannot tell whether a change in the number of galaxies in any particular bin is due to a change in the overall number of galaxies or to the motion of galaxies in and out of that bin from neighboring bins. The latter problem is further exacerbated by the fact that samples are usually size- or brightness-limited and population numbers on the other side of these limits are not known. Finally, uncertain errors can smear counts from one bin to another. All of these problems will be modeled when a full theory of galaxy formation is available to predict how galaxies evolve in every measured parameter. In the meantime, it is hard to break the population into well motivated sub-populations, and we therefore lack the means to obtain more finely divided knowledge.

Amidst this sea of unimodal functions, one function stands out on account of its uniquely bimodal character, namely, the color function. This is visible in the color-magnitude diagram, where early-type E/S0s populate a narrow red sequence that is separated from bluer, star-forming spirals by a shallow valley (Strateva et al. 2001; Hogg et al. 2003; Balogh et al. 2004; Baldry et al. 2004 and references therein). A similar division extends to at least $z \sim 1$ (Im et al. 2002; Bell et al. 2004b; Weiner et al. 2005, Willmer et al. 2005) and possibly beyond (Giallongo et al. 2005). A bimodal distribution is also seen

¹ Based on observations taken at the W. M. Keck Observatory.

² UCO/Lick Observatory, University of California

³ On leave from Observatório Nacional, Rio de Janeiro, Brazil

⁴ Department of Physics, Oxford University

⁵ Department of Physics, University of Maryland

⁶ Lawrence Berkeley Laboratory, Berkeley

⁷ Hubble Fellow

⁸ Astronomy Program, School of Earth and Environmental Sciences, Seoul National University, Seoul, South Korea

⁹ Department of Astronomy, University of California, Berkeley

¹⁰ Department of Astrophysics, Princeton University

¹² Department of Astronomy, University of Texas, Austin

¹³ Department of Physics, Princeton University

¹⁴ Institute for Astronomy, Honolulu

¹⁵ Max-Planck-Institut für Astronomie, Heidelberg, Germany

¹⁶ Department of Physics, National Taiwan University

¹⁷ Astronomy Department, University of Florida

¹⁸ Herzberg Institute of Astrophysics, National Research Council of Canada

¹⁹ Department of Physics, The Johns Hopkins University

²⁰ Department of Astronomy, New Mexico State University

in other parameters such as spectral class (Madgwick et al. 2002, 2003) and morphologies, metallicities, and star formation rates (Kauffmann et al. 2003a,b), but color is by far the easiest to measure. Thus, not only does color sort galaxies cleanly into bins, it is also highly relevant to the emergence of the Hubble sequence.

However, to exploit this opportunity requires highly accurate counts, as the expected effects are not large. For example, counts of red galaxies in the COMBO-17 survey were seen to evolve by only a factor of a few since $z = 1$ (Bell et al. 2004b). Even this small number has vital implications for galaxy formation (see below), but confirming and improving the measurement clearly requires accuracies of order 10-20%. Few previous measurements of distant luminosity functions have attained this accuracy. Red galaxies are especially difficult because of their high clustering, which necessitates large samples over a large number of statistically uncorrelated regions. We are only just now coming to appreciate how formidable the problem of cosmic variance really is (e.g., Somerville et al. 2004)

The present paper addresses these challenges by combining two large surveys, DEEP2 and COMBO-17, to create the largest database yet analyzed of galaxies with $z > 0.8$, containing 39,000 galaxies in total, with 15,600 beyond $z = 0.8$. Further checks are provided by pilot measurements from the DEEP1 survey. The entire sample is large enough and dispersed enough over the sky that cosmic variance and Poisson fluctuations are reduced to 7-15% per redshift bin. The samples were selected and measured in different ways—DEEP2 redshifts are spectroscopic, while COMBO-17’s are photometric—and thus provide an important check on one another. Finally, color bimodality is used to divide red galaxies from blue galaxies at all epochs. The red luminosity function is rederived and compared to the previous results of Bell et al. (2004b, hereafter B04), while the blue function is presented in Paper I and here for the first time (in a sample of this size) and offers a important foil for considering the behavior of the red function. DEEP2 data and COMBO-17 data are found to agree well in all major respects, and the principal conclusions appear to be robust.

Our most important result is to confirm the recent rise in the number of massive red galaxies *at fixed stellar mass* found by B04. In contrast, the number density of massive blue galaxies has remained essentially constant since $z \sim 1$. A second important conclusion is that the characteristic B -band luminosity M_B^* of both red and blue populations has dimmed by about the same factor: we find ~ 1.3 mag per unit redshift for both red and blue populations since $z = 1$. The rise in the number of massive red galaxies implies that most early-type galaxies assumed their final form at relatively late times, below $z = 1$, *where the process can be studied in detail*. The late emergence of spheroidal galaxies disagrees with classic high-redshift, monolithic collapse models for spheroid formation but seems to be consistent with large amounts of other data, as reviewed in §6.

The remainder of this Introduction reviews previous measurements of luminosity functions. The subject has a venerable history (e.g., Binggeli et al. 1988; Tresse 1999; de Lapparent et al. 2003), with determinations ranging from low to high redshift using field and cluster galaxies.

Accurate determinations of local field luminosity functions have finally become available from the 2 Degree Field Galaxy Redshift Survey (2dFGRS, Norberg et al. 2002) and the Sloan Digital Sky Survey (SDSS, Blanton et al. 2003; Bell et al. 2003), providing reliable local benchmarks against which evolution can be measured.

The dependence of the galaxy luminosity function on the internal properties of galaxies has been known since Sandage, Binggeli & Tammann (1985) showed that the shape and magnitude of luminosity functions in the Virgo cluster depend on galaxy morphology and luminosity class. This dependence on internal characteristics is also seen in local field galaxies when morphologies (Marzke, Huchra & Geller 1994; Marzke et al. 1998; Marinoni et al. 1999), colors (Lilly et al. 1995b; Marzke & da Costa 1997; Lin et al. 1999; Blanton et al. 2001) and spectral types (e.g., Heyl et al. 1997; Bromley et al. 1998; Folkes et al. 1999; Cohen 2002; Magdwick et al. 2002; de Lapparent et al. 2003) are considered.

Early studies of the evolution of the galaxy luminosity function to $z \sim 1$ used samples of a few hundred galaxies (e.g., Cowie et al. 1996; Brinchmann et al. 1998; Lin et al. 1999; Cohen 2002; Im et al. 2002; de Lapparent et al. 2003). In a landmark paper using the Canada France Redshift Survey (hereafter CFRS), Lilly et al. (1995b) claimed that the evolution of the luminosity function is coupled to internal properties, being strongly correlated with color and, to a lesser extent, with luminosity. Dividing red from blue galaxies using the median spectral type of the sample, the authors claimed a steepening in faint-end slope for blue galaxies at redshifts beyond $z > 0.5$, while red galaxies showed little change in either luminosity or number density over the redshift range covered, $0.05 \leq z \leq 1$.

A conclusion that evolution depends on internal properties was also reached by Cowie et al. (1996), based on a sample reaching to $z \sim 1.6$. [OII] fluxes were used to estimate star formation rates and K -band photometry to estimate stellar masses. They found that most of the luminosity evolution since $z \sim 1$ is due to blue galaxies with small masses but high star formation rates. More massive galaxies were relatively stable in numbers, particularly in the K -band, while the B -band showed modest number evolution. They concluded that the characteristic mass of galaxies undergoing intense star formation decreases over time, which they termed “downsizing.”

Cohen (2002) measured galaxies in a region centered on the Hubble Deep Field and Flanking Fields and, in contrast to CFRS, found that the luminosity functions of several different spectral classes of galaxies showed no strong evidence of change in faint-end slope to $z \sim 1$, and further that the value of this slope is comparable to the local value. Galaxies with spectra dominated by absorption lines at $z = 1$ were brighter by ~ 1.5 magnitudes relative to local ones, while galaxies with strong [OII] brightened by ~ 0.75 magnitudes at $z \sim 1$.

Im et al. (2002) measured evolution in the luminosity function of morphologically normal red early-type galaxies by selecting distant galaxies to match local E/S0s in both morphology and color. This survey is related to the present work, as it utilized DEEP1 redshifts, supplemented by photo- z ’s. The luminosity function of early-type galaxies showed a brightening of 1.1-1.9 magnitudes in rest-frame B from $z = 0$ to $z \sim 0.8$, but number den-

sity was relatively static over the same epoch. We will have more to say about this work later.

Similar brightening for early-type galaxies was also found by Bernardi et al. (2003) in the Sloan Digital Sky Survey, where a brightening of ~ 1.15 magnitudes per unit redshift back in time was derived based on a sample reaching to $z \sim 0.3$.

In a later study going 2 magnitudes fainter than Im et al., Cross et al. (2004) studied the faint end of the luminosity functions of both red-selected galaxies and morphologically-selected early-type galaxies using ACS images and photometric redshifts. The red-selected luminosity function was found to turn over steeply at faint magnitudes, whereas the morphologically selected sample was flat. The difference was attributed to blue spheroids, which filled in the counts at faint levels in the morphologically-selected sample.

The evolution of the luminosity function as a function of color since $z \sim 1$ was also investigated by Pozzetti et al. (2003), who used the near-infrared-selected K20 survey of Cimatti et al. (2002b) and divided the sample using the color of Sa galaxies. They found a modest rise of at most 30% in the number of red galaxies after $z = 1$ and concluded that most bright red galaxies were already in place by $z \sim 1.3$.

The distant surveys just cited clearly disagree on many points, including the numbers of galaxies, shapes of luminosity functions, and degree of fading over time. However, these early surveys typically cover only a few tens of square arc minutes and in retrospect are seen to be subject to large cosmic variance (see below). More recent surveys containing several thousands of galaxies are just now beginning to provide more robust measurements of the luminosity function. A large survey by Ilbert et al. (2004, VVDS) using the VIMOS spectrograph on the ESO Very Large Telescope has measured the evolution of the total galaxy luminosity function to $z \sim 2$ using a sample of $\sim 11,000$ galaxies to $I_{AB} = 24.0$ with spectroscopic redshifts. The authors find that M_B^* for all galaxies has faded by 1.6 to 2.2 mag from $z = 2$ to $z = 0.05$ but that the number density of all galaxies has remained nearly constant. They also suggest a possible steepening in faint-end slope at $z = 1$.

The DEEP2 Survey (Davis et al. 2003) employs spectroscopic redshifts to measure distances and internal kinematics for $\sim 40,000$ galaxies in four regions of the sky. In order to probe galaxies at redshifts $z \sim 1$, galaxies are pre-selected in three of the regions to have $z > 0.7$ using *BRI* colors. The luminosity function analysis for the first third of the DEEP2 survey is presented in a companion paper to this one by Willmer et al. (2005, hereafter Paper I), which uses $U - B$ color bimodality to study how the luminosity functions of blue and red galaxies change with redshift. The results show significantly fewer blue galaxies with time at fixed absolute magnitude, which is well modeled by a fading in M_B^* together with roughly constant number density. Counts for red galaxies, in contrast, show little change at fixed absolute magnitude and, when fitted with Schechter functions, show a similar fading in M_B^* with time but a formally significant rise in number density.

An alternative strategy to create large samples of galaxies is the use of photometric redshifts. In spite of lower precision, photometric redshifts yield a larger

number of redshifts per unit telescope time and enable distances to be measured for galaxies that are too faint for spectroscopy. This approach has been pursued using both space-based (e.g., Takeuchi et al. 2000; Poli et al. 2001; Bolzonella et al. 2002) and ground-based data (e.g., Fried et al. 2001; Drory et al. 2003; Wolf et al. 2003, hereafter W03; Chen et al. 2003; Gabasch et al. 2004). Of the photometric redshift surveys, the ones most comparable to the present work are COMBO-17 (W03) and the FORS Deep Field (Gabasch et al. 2004, FDF). The latter used a sample of more than 5,500 galaxies down to $I_{AB} = 26.8$ to measure the total reframe *B*-band luminosity function from $z \sim 0.4$ to $z \sim 4$. Like DEEP2 and VVDS, they found a constant number of galaxies back in time but did not find a steepening of faint-end slope despite the fact that their sample goes ten times fainter than VVDS.

COMBO-17 (Wolf et al. 2001, W03) contains $\sim 28,000$ galaxies. Aside from the use of photometric redshifts, it is similar to the DEEP2 survey in terms of depth and coverage. The first luminosity-function analysis of COMBO-17 by W03 divided the sample into bins of fixed spectral type that did not evolve with redshift. Some of the evolutionary trends that were discovered may have reflected color evolution between these fixed spectral bins rather than changes in overall numbers. The approach was changed in a follow-up analysis using the same database by Bell et al. (2004b, B04), who used an evolving color cut based on bimodality to study red galaxies only. As noted earlier, this work obtained the important new result that red galaxies were not only brighter in the past (by > 1 mag) but were also fewer in number, by at least a factor of two at $z = 1$. This claim based on counts was buttressed by a separate argument based on the luminosity density of bright galaxies. This quantity, j_B , can be measured more accurately than either L^* or number density alone and was found to hold roughly constant since $z \sim 1$. Since stellar population models predict a *fading* of red stellar populations by 1–2 mag between $z = 1$ and now (see §5), the total stellar mass bound up in (bright) red galaxies must be *increasing* by about the same factor, providing additional evidence for growth in the red galaxy population since that time.

A specific evolutionary scenario proposed by B04 had the majority of present-day massive E/S0s moving onto the red sequence after $z \sim 1$. The stellar populations of such galaxies would age passively once galaxies were on the red sequence, but individual galaxies would continue to increase their stellar masses via mergers along the sequence, as predicted by the hierarchical model of galaxy formation.

Aside from B04, few works have used color bimodality to measure the luminosity functions of red and blue galaxies separately. One of those that has is by Giallongo et al. (2005), who used a mixture of deep and shallow data in four fields containing 1,434 galaxies. Dividing galaxies both by $U - V$ color and by star-formation rate, they found that color bimodality persists to $z \sim 2$ but that the number density of red galaxies drops steeply beyond $z = 1$. They do not give numbers for $z = 1$ specifically, which makes quantitative comparison with our results difficult, but our conclusions below agree at least qualitatively with theirs.

The foregoing summary illustrates that information on

distant luminosity functions is still fragmentary and often contradictory. In particular, the claim by Bell et al. (2004b) for the emergence of red galaxies after $z = 1$ has not yet been checked. A major impediment is cosmic variance—many of the above samples, especially the early and/or deepest ones, cover only a few tens of square arc min, for which the rms cosmic variance is $\sim 50\%$ per $\Delta z = 0.2$ at $z = 1$, being even greater for red galaxies (Somerville et al. 2004). Since number-density evolution by factors of two or three is at issue (B04), definitive results cannot be obtained using such small areas, and larger samples are needed. DEEP2 and COMBO-17 fill that need; each sample is large enough on its own to give statistically meaningful results, thus providing significant checks on one another.

The paper is organized as follows: §2 presents the data, which include not only COMBO-17 (W03) and DEEP2 (Paper I) but also data from the smaller DEEP1 pilot survey, which are presented here for the first time. §3 briefly summarizes methods used to measure the luminosity functions and their evolution, referring the reader to Paper I and W03 for more details. Readers wanting results quickly can skip directly to §4, which presents the luminosity functions, computes values of M_B^* , number density, and j_B from fitting to Schechter functions, and compares the answers to local and distant values from the literature. These are our core results on evolution. A detailed discussion of possible sources of error is presented in §5, which can also be skipped on first reading. The implications for galaxy formation, especially of red galaxies, are discussed in §6, which draws heavily on the properties of local E/S0s as well as distant ones. We ultimately favor a stepwise, “mixed” scenario in which (massive) E/S0s are quenched during a final gas-rich merger event, migrate to the red sequence, and then undergo a small number of further, purely-stellar mergers on the red sequence to attain their final masses. This scenario is similar to the one outlined by B04 and seems to have the right mixture of ingredients to explain the boxy-disk “structure sequence” of local ellipticals plus the narrow E/S0 scaling relations and the age- Z anticorrelation that underlies them. Speculation on the nature of the quenching mechanism and its possible downsizing over time ends the discussion. A final summary is presented in §7.

Throughout this work, a $(H_0, \Omega_M, \Omega_\Lambda) = (70, 0.3, 0.7)$ cosmology is used. Unless indicated otherwise, all magnitudes and colors are on the Vega system. Necessary conversions to AB magnitudes are given for reference in Table 1 of Paper I. Luminosity functions are specified per unit co-moving volumes.

2. DATA

The main data analyzed in this paper come from the DEEP2 and COMBO-17 surveys, with supporting data from DEEP1. Detailed background information on these surveys appears in other references, but core information needed to understand the samples and their selection effects is provided below. Basic properties of the surveys (area, number of galaxies, magnitude and redshift limits) are summarized in Table 1.

2.1. DEEP2

The DEEP2 survey strategy, data acquisition, and data reduction pipeline are described in Davis et al. (2003), Faber et al. (in prep.), and Newman et al. (in prep.). A detailed summary was provided in Paper I as background to computing the DEEP2 luminosity functions; the functions from Paper I are adopted here without change. DEEP2 catalogues are derived from Canada-France-Hawaii Telescope images taken with the $12K \times 8K$ mosaic camera (Cuillandre et al. 2001) in B , R and I in four different regions of the sky. Reduction of the photometric data, object detection, photometric calibration, and construction of the star-galaxy catalogs are described in Coil et al. (2004). R -band images used to define the galaxy sample have a limiting magnitude for image detection at $R_{AB} \sim 25.5$. Apparent-magnitude cuts of $R_{AB} \geq 18.5$ and $R_{AB} \leq 24.1$ and a surface brightness cut of $\Sigma_R \leq 26.5$ were applied (see Paper I). Separation between stars and galaxies is based on magnitude, size, and color, which were used to assign each object a probability of being a galaxy; star-galaxy separation efficiency is discussed in Coil et al. (2004) and Paper I. In Fields 2, 3, and 4, the spectroscopic sample is pre-selected using B , R , and I to have estimated redshifts greater than 0.7, which approximately doubles the efficiency of the survey for galaxies near $z \sim 1$. The fourth field, the Extended Groth Strip (EGS), does not have this pre-selection applied but instead has roughly equal numbers of galaxies below and above $z = 0.7$, which were selected using a well understood algorithm versus redshift. Redshifts were measured spectroscopically using the DEIMOS spectrograph (Faber et al. 2003) on the Keck 2 telescope. Slitlets are placed (nearly) randomly on 50% of all galaxies after pre-selection (70% without pre-selection in EGS), of which 70% yield successful redshifts (80% in EGS), with a catastrophic failure rate of 1%.

The DEEP2 sample used here combines data from the first season of observations in Fields 2, 3, and 4 with 1/3 of the total EGS data, which provides an initial sample at low redshifts. The total number of galaxies is 11,284, with 4,946 (44%) in EGS, 3948 (35%) in Field 4, 2299 (20%) in Field 3, and 91 (1%) in Field 2. Since the photometric redshift cut at $z \sim 0.7$ provides a soft boundary for the selection of galaxies, only EGS is used to probe the lower-redshift realm $z < 0.8$, while data in all four fields are used for $z \geq 0.8$. Color-magnitude diagrams illustrating the sample binned by redshift are shown in Paper I.

2.2. COMBO-17

The COMBO-17 survey consists of multi-color imaging data in 17 optical filters covering a total of $1 \square^\circ$ of sky at high galactic latitudes. The filter set contains five broad-band filters ($UBVRI$) plus 12 medium-band filters stretching from 400 to 930 nm. All observations were obtained with the Wide Field Imager (WFI, Baade et al., 1998, 1999) at the MPG/ESO 2.2-m telescope on La Silla, Chile. The total exposure time is ~ 160 ksec per field, which includes a ~ 20 ksec exposure in the R -band with seeing below $0''.8$ FWHM. The WFI provides a field of view of $34' \times 33'$ on a CCD mosaic consisting of eight $2K \times 4K$ CCDs with ~ 67 million pixels providing a scale of $0''.238/\text{pixel}$. The observations began during the commissioning phase of the WFI in January 1999

and are continuing as the area is extended to cover more fields. The data used here are from three fields covering an area of $0.78 \square^\circ$, providing a catalogue of $\sim 200,000$ objects found by SExtractor (Bertin & Arnouts 1996) on R -band images with a $5\text{-}\sigma$ point-source limit of $R \sim 26$.

SEDs created from these 17 passbands were used to classify all objects into stars, galaxies, and QSOs by comparison with template SEDs. Less than 1% of the sources have spectra that are peculiar, not yielding an object class (W03), and star-galaxy separation is highly efficient. A first analysis of the COMBO-17 luminosity function was published by W03, but the galaxy catalogue has changed slightly since then. Basic details of the classification algorithm and choice of templates were given in Wolf, Meisenheimer & Röser (2001). In 2003, an improved set of SED templates was introduced after it was found that the accuracy of galaxy redshifts was limited by template mismatch for bright galaxies, for which more subtle SED details could be seen. The new set of galaxy templates contains a grid of synthetic spectra based on the PEGASE code for population synthesis models (Fioc & Rocca-Volmerange 1997), whereas in the past the redshift determination relied only on the observed templates by Kinney et al. (1996). The new redshifts are accurate to within $\delta z/(1+z) < 0.01$ at $R < 21$ and to within 0.05 down to $R < 24$ (Wolf et al. 2004, hereafter W04). The changes from the old redshifts are relatively small (see Figure 4 in W04) and are within the errors of the old estimates, but residual errors were reduced by up to a factor of 3 for galaxies with selected SED shapes. Typical catastrophic failure rates for COMBO-17 galaxies are $\sim 1\%$ in the magnitude range used for the LFs, as measured using galaxies in common between W04 and Le Fèvre et al. (2004) in Chandra Deep Field South. The resulting luminosity functions of galaxies are also unchanged within the errors published in W03 if the same color divisions are used. The luminosity functions of red-sequence galaxies published by B04 were already based on the new redshift catalogue.

In this paper, we recalculate luminosity functions from the COMBO-17 galaxy sample using different color divisions than before. The red-sequence cut is similar to the one in B04, with a small difference: B04 measured the mean color of the red-sequence, which is affected to a small degree by K-correction errors that vary in a non-stochastic way with redshift. They then fitted a smooth evolution to the measured colors to identify the most likely trend. Here we use the measured red-sequence colors in each individual redshift bin to define the color valley, and thus the cut. As stated by B04, the difference this makes to luminosity functions is small. However, we consider it preferable to follow the small but systematic variations in the data for the purpose of splitting the population. The new method is identical to that used for DEEP2 (see Paper I).

In COMBO-17, a galaxy redshift measurement is considered successful when the error expected from the probability distribution is below a threshold of $\sigma_z/(1+z) \lesssim 0.1$. The completeness of successful redshifts depends on galaxy rest-frame color, and simulated completeness maps are shown in W03 and W04. The large redshift incompleteness among blue galaxies at the faint end of the COMBO-17 sample would lead to unreliable completeness corrections in the last few LF bins just above the

survey limit. These bins have thus been dropped, and all correction factors used in the remaining bins (plotted data points) are below 1.5. For red-sequence galaxies at $z < 1.2$, which are the special focus of this paper, redshifts are measured successfully for the *entire* sample at $R < 24$ used for the luminosity function. This claim can be tested by identifying likely red-sequence galaxies from an apparent color-magnitude diagram like that in Figure 1a. In COMBO-17, galaxies with failed redshifts occupy solely the region of blue galaxies. This is consistent with (a) the known lower COMBO-17 completeness for redshifts of blue galaxies close to the faint limit, and (b) the zero completeness (by design) of COMBO-17 with respect to $z > 1.4$ galaxies. Blue galaxies with $z > 1.4$ are expected to be a much larger part of a flux-limited sample with $R < 24$ than red-sequence galaxies at $z > 1.4$. Owing to their red colors and faint near-UV fluxes, only red-sequence galaxies of extremely high luminosity could pass the flux limit at high redshift, of which there are evidently very few.

2.3. DEEP1

DEEP1 was a pilot survey for DEEP2 that was conducted using the LRIS spectrograph on the Keck telescopes in 1995-1999. Since the only published luminosity function using DEEP1 data treated E/S0s (Im et al. 2002) above $I814 = 22$, a more detailed description of DEEP1 data will be presented here. This summary also serves to convey the flavor of our treatments of DEEP2 and COMBO-17. Readers not interested in these details should skip to §3.

Background on DEEP1 sample selection and photometry is presented in Vogt et al. (2005), on photometry and bulge-disk decompositions by Simard et al. (2002), and on spectroscopy and redshifts by Weiner et al. (2005). The DEEP1 sample is drawn from objects detected in a set of 28 contiguous Wide Field and Planetary Camera (WFPC2) Hubble Space Telescope pointings at approximately $14^h 16^m 30^s +52^\circ 15' 50''$ (J2000.0), (PIs E. Groth, GTO 5090; and J. Westphal GTO 5109). The solid angle covered by the GSS is 127 square arc minutes.

The DEEP1 photometric catalogue was created by Groth et al. (1994) and contains several parameters measured using FOCAS (Tyson & Jarvis 1981). To this catalogue were added total magnitudes and colors measured fitting 2-dimensional bulge+disk models using the GIM2D package (Simard et al. 1999, 2002). For galaxies without GIM2D measurements, magnitudes and colors measured by Ratnatunga et al. (1999, MDS) in the Medium Deep Survey were used, which were shown by Simard et al. (2002) to have comparable quality to GIM2D measurements. When neither GIM2D nor MDS had magnitudes and colors, the FOCAS measurements were transformed into the same system as the GIM2D magnitudes by adding the median offset between GIM2D and FOCAS magnitudes in each color ($I814 = I_{FOCAS} - 0.295$ and $V606 - I814 = (V - I)_{FOCAS} + 0.106$) (all HST magnitudes are on the Vega system.)

DEEP1 spectroscopic data were obtained over several observing runs using the Low Resolution Imaging Spectrograph (LRIS, Oke et al. 1995) on the Keck 1 and 2 telescopes. Most galaxies were observed using two different gratings, with a blue side ranging from 4500 Å to 6500 Å and a red side from 6000 Å to 9500 Å. Total exposure

times ranged from about 50 minutes for galaxies observed on one mask up to ~ 500 minutes for galaxies placed on several masks. In the analysis below, the DEEP1 sample is restricted to galaxies with $16.5 \leq I814 \leq 23.5$ and with redshift quality A or B, as explained in Weiner et al. (2005) (no surface-brightness cut was applied). Galaxies generally have more than one identified spectral feature, and the redshift confidence level is better than 90%. The total number of galaxies in the region that satisfy the apparent magnitude limit is 2,438, of which 621 have good quality redshifts. The typical sampling rate of DEEP1 redshifts is $\sim 40\%$, and the typical redshift success rate is $\sim 70\%$, for a final overall sampling density of $\sim 25\%$.

The apparent color-magnitude diagram of DEEP1 galaxies is shown in Figure 1. The spectroscopic sample was selected from a “pseudo- R ” band magnitude: $[(V606 + I814)/2 \leq 24.0]$; this has been converted to an approximate $I814$ magnitude shown as the vertical dotted line in all four panels. Figure 1a shows the full sample of galaxies, and Figure 1b shows the distribution of galaxies placed in slits. Because of the R -band selection, shown as the inclined dashed line, there is a dearth of red galaxies fainter than $I814 = 23.5$; brighter than this, the sample of galaxies placed on masks is a good representation of the total galaxy sample. Figure 1c presents the distribution of galaxies that were successfully measured; green symbols show galaxies below the adopted high- z cutoff (see below), while red symbols show galaxies beyond the cutoff, which were not used. Black crosses show galaxies with redshifts from CFRS (Lilly et al. 1995b) and from Brinchmann et al. (1998), for which DEEP1 measured no spectrum. Figure 1d shows the distribution of galaxies with failed redshifts. The few bright cases of failed redshifts resulted from short integrations or spectra of galaxies at mask edges, while the majority of failures are of faint and generally blue galaxies. As in DEEP2 and COMBO-17, most failures are likely beyond the adopted high-redshift cutoff of the survey, here taken to be $z_h = 1.0$. This is the cutoff for the DEEP1 analysis and is the redshift where O II $\lambda 3727$ becomes heavily confused with strong OH sky lines in the LRIS data (Weiner et al. 2005).

Figure 2 divides the apparent color-magnitude diagram into magnitude and color bins. For each bin, the histogram of the distribution of galaxies as a function of redshift is shown, where the filled histogram represents successful measures and the open bar at the right the number of failures inside each bin. The number of failed redshifts increases at magnitudes fainter than $I814 \sim 22.5$.

Figure 3 shows the distribution of restframe $U - B$ vs. redshift. The method used to measure $U - B$ is described in Weiner et al. (2005), using the procedure described in Paper I but limited to the two observed filters ($V606$ and $I814$). A bimodal color distribution is clearly seen, as well as large-scale structure fluctuations due to galaxy clustering (vertical stripes). The number of successful redshifts above $z = 1$ falls drastically owing to OH confusion (see above).

Rest-frame color-magnitude diagrams for different redshift intervals are shown in Figure 4. Similar diagrams for DEEP2 were shown in Paper I and for COMBO-17 in B04. The solid line in each panel represents the limiting absolute magnitude that corresponds to apparent magnitude $I814 = 23.5$ at the far edge of the bin as a function

of restframe color. The color dependence was calculated using the K-correction code from Paper I. The changing slope of the line as a function of redshift is caused by the fact that the $I814$ -band filter used to select the sample coincides with rest B at $z \sim 0.8$ but differs from it increasingly as the redshift is either greater or smaller than 0.8. Intrinsically red galaxies are included to fainter absolute magnitudes when observed $I814$ is redder than rest B , while intrinsically blue galaxies are favored when observed $I814$ is bluer than rest B , thus causing the line to swing with redshift.

The upper dashed line in each figure represents the cut used to separate red from blue galaxies. This cut is identical to that used by Paper I for DEEP2 since the restframe colors and magnitudes are on the same system. The equation for the line is

$$U - B = -0.032(M_B + 21.52) + 0.454 - 0.25, \quad (1)$$

which is taken from the van Dokkum et al. (2000) color-magnitude relation for red galaxies in distant clusters, converted to the cosmological model used in this paper, and corrected downward by 0.25 mag in order to pass through the valley between red and blue galaxies (Paper I). Although the colors of red galaxies may evolve with redshift, this effect is not strongly seen in either DEEP1 or DEEP2 colors, and a line with constant zero point independent of redshift is used for all redshift bins.

We conclude this section by comparing the strengths and weaknesses of the two major data sets used in this paper, DEEP2 and COMBO-17. Both data sets go to nearly the same apparent magnitude, $R \sim 24$, and have comparable numbers of galaxies beyond $z = 0.8$ (see Table 1). The square root of cosmic variances are shown for each sample in Tables 2-4 by galaxy color and by redshift bin. They are comparable for the two surveys beyond $z = 0.8$ and range between 10-20% for all redshifts and color classes. When combined, the two surveys have a total (square root) cosmic variance of ~ 7 -15% per redshift bin at $z \sim 1$. The strengths of DEEP2 are rock-solid redshifts and high completeness for blue galaxies all the way to $z = 1.4$ owing to the sensitivity to [O II] $\lambda 3727$, which is strong in distant blue galaxies. The strengths of COMBO-17 are higher completeness overall at all redshifts, particularly for distant red galaxies near $z \sim 1$. This is offset by a tendency to lose redshifts for blue galaxies towards the faint limits of the survey, which has forced us to cut off the COMBO-17 All and Blue luminosity functions at a shallower point than DEEP2 to keep completeness corrections small. The two data sets thus complement each other well at high z , making a parallel, head-to-head analysis extremely useful.

3. METHODS

The luminosity function is most frequently expressed using the Schechter (1976) parameterization, which in magnitudes is:

$$\phi(M)dM = 0.4 \ln 10 \phi^* 10^{0.4(M^* - M)(\alpha + 1)} \{-10^{0.4(M^* - M)}\} dM, \quad (2)$$

where ϕ^* is a normalizing constant that is proportional to the total number density of galaxies, and α is the slope of the power law that describes the behavior of the faint end of this relation. Changes in these parameters with time quantify how galaxy populations evolve.

The methods used for the DEEP2 (and DEEP1) luminosity functions are described in Paper I. The methods used for COMBO-17 are described in W03 and are very similar. A brief overview of all methods is provided here.

Two statistical estimators have traditionally been used in the calculation of the luminosity function. These are the parametric maximum-likelihood method of Sandage, Tammann & Yahil (1979, STY; also Efstathiou, Ellis & Peterson 1988; and Marzke, Huchra & Geller 1994) and the non-parametric $1/V_{max}$ method of Schmidt (1968; also Felten 1976 and Eales 1993). The STY method fits an analytic Schechter function, yielding values of the shape parameters L^* and faint-end slope α , but not the density normalization ϕ^* , which is estimated using the minimum-variance density estimator of Davis & Huchra (1982). The STY method also does not produce any visual check of the fit. In this paper, a visual check both on shape and normalization for each redshift bin is obtained using $1/V_{max}$ since it yields the average number density of galaxies in bins of redshift and absolute magnitude. Formulae used for obtaining the STY parameters, $1/V_{max}$ points, and the density normalizations are given in Paper I.

Since the STY method does not yield ϕ^* , it is not suitable for calculating the correlated errors between ϕ^* and M^* . For DEEP, these errors were calculated from the $1-\sigma$ error ellipsoid (Press et al. 1992) that results from fitting a Schechter function to the $1/V_{max}$ data points (Paper I). Although the luminosity functions obtained from the STY and $1/V_{max}$ methods are not quite identical (see Figure 6 below), the differences are small and errors from the $1/V_{max}$ method should also apply to the STY method. For COMBO-17, the errors in parameters were calculated first for M_B^* using STY, and then the ϕ^* errors were calculated using the field-to-field variations (W03).

Weights are needed for every data set to correct for missing galaxies. The adopted weights need to take into account the fact that 1) objects may be missing from the photometric catalogue, 2) stars may be identified as galaxies and vice versa, 3) not all objects in the photometric catalogue are targeted for redshifts, and 4) not all targets yield successful redshifts. For the DEEP surveys, factors 1) and 2) are small or zero (see discussion in Paper I), and only factors 3) and 4) need to be taken into account. The basic assumption to deal with 3) is that all unobserved galaxies share the same average properties as the observed ones in a given color-magnitude bin. Factor 4) is dealt with by assigning a model redshift distribution to the failed galaxies. We use two such models, as explained in Paper I. The “minimal” model assumes that all failed galaxies lie entirely beyond the high-redshift cutoff of the survey, which is $z_h = 1.4$ for DEEP2 and $z_h = 1.0$ for DEEP1. As discussed in Paper I, this model should provide an adequate description for blue galaxies. The second model to treat failed redshifts is the “average” model, which assumes that failed redshifts have the same distribution as the successful redshifts in the same color-color-magnitude bin; this is a reasonable assumption for red galaxies. The difference in weights between the minimal and average models is usually $\leq 25\%$ (average weights are higher), and most of the large differences occur for galaxies with extreme colors at faint magnitudes. Luminosity functions calculated with the average

model are slightly higher than those using the minimal model, by an amount that averages 10-20%. When the combined All-galaxy sample is considered, we use an “optimal” model in which red galaxies are modeled using the average model and blue galaxies are modeled using the minimal model.

Two small alterations to this general scheme were applied. In the case of EGS in DEEP2, a final correction (described in Paper I) was applied to account for the different sampling strategy used in this field, which includes low-redshift galaxies but de-weights them so that they do not dominate the sample. In the case of DEEP1, the weights were modified to use additional size information from HST images, which show that *all* galaxies with angular half-light radius $r_{hl} \geq 1$ arc sec (from GIM2D) lie within the legal redshift range $z \leq 1.0$. Figure 5 illustrates these results for DEEP1 by plotting sampling rates, redshift-success rates, and weights; analogous figures are given for DEEP2 in Paper I.

For the COMBO-17 survey, effect 1) from the list above is small, as only galaxies very close to very bright stars are lost from the object catalogue. Effect (3) is zero, as the photo- z code works on the entire catalogue. Effects (2) and (4) are linked, since in COMBO-17 both object classification and redshift estimation are one single process. In one direction, a few K stars are misidentified as galaxies, but their number is negligible. In the other direction, the misclassification of galaxies as stars is modeled together with redshift incompleteness using simulations as described in Wolf et al. (2001) and W03, which take into account the photometry S/N, SED, and redshift and are calibrated using Monte-Carlo simulations. Weights are calculated as a function of apparent magnitude and color and are close to unity for all red galaxies, for which we calculate the luminosity to the full sample depth, but drop rapidly for blue galaxies towards the survey limit. We have not used any data points that involve corrections by more than a factor of 1.5, and as a result the COMBO-17 luminosity function points for the Blue and All samples do not quite reach luminosities corresponding to apparent magnitude $R = 24$.

4. ANALYSIS

4.1. The DEEP and COMBO-17 Luminosity Functions

This section compares the luminosity functions derived from DEEP2, DEEP1, and COMBO-17 with one another and with published data. The DEEP2 functions are best estimates from Paper I that use the optimal missing-redshift model for All galaxies, minimal for Blue galaxies and the average model for Red galaxies (see §3). For the DEEP1 sample we use the minimal model for all galaxy colors, while COMBO-17 weights are as described in §3 and W03. Galaxies are analyzed all together (the “All” sample) and divided into “Red” and “Blue” sub-samples using color-magnitude bimodality. The method used to divide blue and red galaxies in DEEP2 and DEEP1 is based on the slanting line that goes through the color valley in the $U - B$ vs. M_B CM diagram (see Equation 1 and Figure 4). The line used for COMBO-17 is similar to the one used by B04 based on $U - V$ vs. M_V except that the smoothly-evolving zero point of the line through the color valley is replaced by a zero point adjusted in each redshift bin to make the line go through the valley at that redshift.

Figure 6 shows the resulting luminosity functions for the All data (top row), Blue data (middle row), and Red data (bottom row). Redshift increases from left to right across a row. Non-parametric $1/V_{max}$ data points are shown for DEEP2 by the solid black squares, for DEEP1 by the grey triangles, and for COMBO-17 by the red circles. For all samples, the calculation of the luminosity function is truncated at the faint end using dashed lines analogous to those in Figure 4, taking the limiting absolute magnitude at each color and in each redshift bin into account; details are given in Paper I. Blue galaxies were further trimmed in COMBO-17 as described in §3, to allow for greater redshift incompleteness.

The error bars on each DEEP2 and DEEP1 point represent Poisson statistics only. Cosmic variance estimates are shown as the separate error bar at the top left corner of each panel and were estimated using the procedure of Newman & Davis (2002) to account for evolution of the correlation function. The bias factors derived by Coil et al. (2004) for red galaxies ($b = 1.32$) and blue galaxies ($b = 0.93$) relative to dark-matter halos are included in these estimates. The values plotted are for DEEP2. To first order, Poisson variance is random from point to point, whereas cosmic variance should mainly move all points in a given bin up and down together. Since these effects are different, they are shown separately. For COMBO-17, the error bars combine the Poisson errors in $\phi(M)$ with the cosmic variance estimated from the field-to-field variations.

Also shown in the top row of Figure 6 are $1/V_{max}$ data points by Ilbert et al. (2004, VVDS), represented by blue diamonds. This sample uses $\sim 11,000$ spectroscopic redshifts from the VVDS survey to $I_{AB} = 24$ (7,800 redshifts are termed “secure”). Finally, the grey dashed lines show Schechter fits to local red and blue SDSS samples at $z \sim 0.05$ from Bell et al. (2003), who divided galaxies both by color and by concentration, getting similar results. The exact Schechter parameters used are given in Table 5.

The conclusions from Figure 6 are as follows:

All galaxies (top row): Measurements of the All-galaxy luminosity function from all four surveys agree well out to $z \sim 1$ and down to the apparent magnitude limit of DEEP2 and COMBO-17 ($R \sim 24$). Below this, VVDS claim to see a steepening in faint-end slope from $\alpha \sim -1.2$ at $z = 0.05$ to $\alpha \sim -1.5$ at $z = 1$. Neither DEEP2 nor COMBO-17 go deep enough to test this, but, as noted above, Gabasch et al. (2004, FDF) go nearly 2.5 magnitudes fainter and do not see it, getting $\alpha = -1.25$ at all redshifts. Relative to the local Schechter total function, the data in successive redshift bins march to dimmer magnitudes (M_B^*) with time but stay roughly constant in number density (ϕ^*). This visual assessment is confirmed by Schechter fits below. In short, for the population as a whole (All sample), galaxies are getting dimmer with time but their number density has remained much the same, since $z \sim 1$.

Blue galaxies (middle row): The results found above for the All sample are replicated for the Blue sample, as expected since blue galaxies account for the majority of objects at all redshifts. Results here are available only from DEEP1, DEEP2, and COMBO-17 since VVDS do not divide their samples by color. However, these three data sets agree well. Relative to the local blue Schechter

function (dashed grey line), M_B^* dims with time while ϕ^* remains constant, again confirmed by Schechter fits below.

Red galaxies (bottom row): Before considering red galaxies, we review the conclusions of Bell et al. (2004b, B04), which offered the first analysis of evolution in ϕ^* and M_B^* for red galaxies, based on COMBO-17. The main finding was that M_B^* for red galaxies dims over time by ~ 1.5 mag from $z = 1$ to 0 and that ϕ^* rises by at least a factor of two. This evidence for evolution from the luminosity function was further bolstered by consideration of the total B -band luminosity density of red galaxies, j_B , which is measured with smaller (formal) errors than M^* or ϕ^* separately. The quantity j_B was found to hold nearly constant since $z = 1$. Since models of stellar evolution for red galaxies predict a rise in B -band stellar mass-to-light ratio by 1-2 mag since $z = 1$ (see more on this below), constant j_B implies that the total stellar mass contained in red galaxies has at least doubled since $z = 1$, providing further evidence for significant growth and change in red galaxies over this epoch.

Bell et al.’s finding of recent strong evolution among red galaxies disagrees with the classic scenario for red-galaxy formation in which E/S0 galaxies assembled their mass and formed stars very early and have been passively fading ever since (e.g., Eggen, Lynden-Bell & Sandage 1962; Larson 1975). The monolithic-collapse picture predicts constant ϕ^* accompanied by equal dimming in both M_B^* and j_B , but neither of these trends was seen by B04. Checking these conclusions by remeasuring these quantities with both DEEP2 and COMBO-17 was therefore a major goal of the present study.

The bottom row of Figure 6 presents the new data for red galaxies. As before, DEEP2 and COMBO-17 agree well. The most striking impression is the relative *lack* of evolution in the red luminosity function, especially when compared to the large shift to brighter magnitudes seen in the blue function. What evolution there is quantified below by Schechter fits, which are shown in Figure 6 as the black lines. These fits indicate a formal dimming of M_B^* over time, accompanied by a rise in number density, ϕ^* . The sense of these shifts is such that the data translate *nearly parallel* to themselves, leaving the raw counts at a fixed absolute magnitude relatively constant. Since the actual counts are not changing a great deal, to first order, the fitted values of M_B^* and ϕ^* must depend on slight curvature signals in the data, which could be weak and unreliable. We return to this question below, where the relative constancy of the red counts is considered from various points of view. For now we simply note that both the raw data and the fitted Schechter function parameters from DEEP2 and COMBO-17 agree extremely well, and that the *formal* values of ϕ^* from both data sets agree with the rise found by B04.

Another important result in Figure 6 is the marked *turnover* in the slope of the Red luminosity function at the faint end. This turnover is well established in both DEEP2 and COMBO-17 at intermediate redshifts and is seen by Cross et al. (2004) and by Giallongo et al. (2005) at even higher redshifts. However, DEEP2 and COMBO-17 may disagree with one another in the lowest redshift bin ($z = 0.2-0.4$), where the number of faint red galaxies continues to turn over according to DEEP2

but flattens according to COMBO-17. This is noteworthy as only the potential discrepancy between DEEP2 and COMBO-17, but the error bars on COMBO-17 are large, reflecting large field-to-field variations. Other data sets have also yielded conflicting values for the nearby red faint-end slope. For example, by identifying early-type galaxies in SDSS using both concentration and color, Bell et al. (2003) found only a modest turnover at the faint end, as in COMBO-17, whereas Madgwick et al. (2002) identified red galaxies spectroscopically in 2dF and found a strong turnover, more like DEEP2 (see Table 2). The question of the red faint-end slope and its possible evolution with redshift is very important for understanding the processes that created red-sequence galaxies. We return to this question in §5 below when discussing errors in the Schechter function parameters caused by possible evolution in the red faint-end slope versus redshift.

In passing, we note the grey triangles in Figure 6, which show luminosity functions from DEEP1. These agree rather well with the functions from DEEP2 and COMBO-17 except in bin $z = 0.8 - 1.0$, where total DEEP1/Red is a factor of 1.5 too high. Two “walls” due to large-scale structure appear in that redshift bin, one at $z \sim 0.81$ and a larger one at $z \sim 0.98$ (Le Fèvre et al. 1994; Koo et al. 1996; see also Figure 7). However, the observed fluctuation is not much larger than the expected cosmic variance limits ($\sim 30\%$).

4.2. Schechter Fits

This section presents the results of fitting Schechter functions to DEEP2 and COMBO-17 using the STY method. Aside from the possible low-redshift flattening of the Red function in COMBO-17, we see no variations in faint-end slopes that are statistically significant in different redshift bins, motivating the use of constant values of α obtained from averaging over several bins. (In fact, small changes are expected in the shape of the All galaxy function with redshift because the shapes of the Red and Blue functions differ and their relative numbers are changing with redshift; however, this effect is small.) We decided to average the faint-end slope values found within the range $z = 0.2$ to 0.6 for COMBO-17 (because of its larger number of galaxies in this redshift range), which yielded $\alpha = -0.5$ for the Red sample and $\alpha = -1.3$ for the All and Blue samples (these values were also used for DEEP2 in Paper I). The latter slope agrees well with the value $\alpha = -1.25$ found for all galaxies by FDF, while the former is close to the average value -0.59 found for distant red galaxies by Giallongo et al. (2005).

Schechter function parameters for both DEEP2 and COMBO-17 are presented in Table 2 for the All sample and in Tables 3 and 4 for the Blue and Red samples. Column (1) shows the central redshift of the bin; column (2) the number of galaxies used in the luminosity function calculation in each redshift bin; column (3) the value of the adopted faint-end slope α ; column (4) the value of M_B^* , followed by the upper and lower 68% errors in columns (5) and (6); the mean density ϕ^* is given in column (7), followed by the 68% errors in columns (8) and (9); the square root of the cosmic variance error is shown in column (10); and the luminosity density (see §4.3), followed by the 68% errors in columns (11) and (12). Column (13) indicates the the weighting scheme described in §3.3 adopted for the DEEP2 fits. As

explained above, we adopted minimal weighting for the DEEP2 Blue sample and average weighting for the Red sample because we think that failed redshifts in the two color classes have different redshift distributions. The All sample combines each of these populations with its preferred weighting scheme (called “optimal” in Table 2).

For DEEP2, the 68% errors are Poisson estimates for M_B^* and ϕ^* and are taken from the $\Delta\chi^2 = 1$ contour levels in the (M_B^*, ϕ^*) plane, computed from the $1/V_{max}$ residuals and their errors. Errors for j_B are conservatively calculated by adding the fractional Poisson errors for M_B^* , ϕ^* , and cosmic variance in quadrature; these latter are overestimates because they neglect correlated errors in M_B^* and ϕ^* , which tend to conserve j_B . However, since the biggest error term is usually cosmic variance, the overestimate is small. For COMBO-17, the 68% errors in M_B^* , ϕ^* , and j_B are rms estimates from field-to-field variations, which are particularly large for the redshift bin centered at $z = 0.9$, caused by a big downward fluctuation in CDF-South. The tabulated cosmic variance errors estimates for both samples were computed as described above for DEEP2, taking the volume and field geometries into account and using separate bias (b) values for All, Blue, and Red galaxies.

The resulting Schechter fits for DEEP2 are shown as the solid black lines in Figure 6. All fits use only the magnitude ranges of the data actually shown. The close match between the fitted curves and all data suggests that the Schechter formula, and in particular the assumed α values, are a good match to the luminosity function shapes over the magnitudes ranges where the data exist. The match of the Schechter form to red galaxies was explored quantitatively in Paper I and is reviewed again under errors in §5.

Evolutionary trends in fitted Schechter function parameters are shown in Figure 7. Besides DEEP2 and COMBO-17, this figure adds data from other recent surveys (2dF [Norberg et al. 2002, Madgwick et al. 2002]; SDSS [Blanton et al. 2003, Bell et al. 2003]; VVDS [Ilbert et al. 2004]; FDF [Gabasch et al. 2004]; DEEP1 [Im et al. 2002]). For reference, the parameters from these surveys are tabulated in Table 5. Since the various surveys use different values for α , changing them to the same values used by DEEP2 and COMBO-17 would cause small shifts in M_B^* and ϕ^* . For example, if local All and Blues values were corrected to match DEEP2 and COMBO-17, M_B^* would brighten by ~ 0.2 mag, and ϕ^* would decline by ~ 0.1 dex; these would act to *reduce* the gaps visible in Figure 7 between the local and distant values. For red galaxies, the changes are opposite: M_B^* would dim by ~ 0.15 mag while ϕ^* would increase by ~ 0.08 dex, acting to *increase* the gaps. All these corrections are small but add somewhat to the uncertainties.

Figure 7 contains the principal results of this paper. The first conclusion (from the top row) is that M_B^* has dimmed for all galaxies, and by roughly the same amount for All, Blue, and Red samples. COMBO-17 (red circles) agrees well with DEEP2 (black squares) in all three color bins, and VVDS and FDF agree well with them for All galaxies (the latter do not subdivide by color). The level of agreement is impressive because the samples were selected and measured in very different ways: COMBO-17 and DEEP2 are R -band selected to $R = 24$, VVDS is I -band selected to $I_{AB} = 24$, and FDF is I -

band selected to $I_{AB} = 26.8$. VVDS and DEEP2 use spectroscopic redshifts, COMBO-17 uses high-precision photometric redshifts based on 17 filters, and FDF uses photo- z 's derived from photometry in 9 bands including J and K . Despite these differences, values of M_B^* for all four distant surveys typically agree to within ± 0.1 mag. Agreement for the two local surveys as analyzed by Bell et al. (2003, SDSS) and Norberg et al. (2002, 2dF) is also good (though Blanton et al. (2003) find SDSS M_B^* dimmer by 0.4 mag). In short, a consistent picture for the evolution of M_B^* for all galaxies since $z = 1$ is emerging.

The dashed grey lines in the top row are an attempt to fit straight lines to M_B^* versus redshift using all the data. It is not clear that this is advisable since the All data in particular seem to show a leveling out in M_B^* at intermediate redshifts. If this is ignored, the coefficients (in Table 6) show that the total dimming in M_B^* to $z = 1$ is 1.30 ± 0.20 mag for the Red sample, 1.31 ± 0.14 mag for the Blue sample, and 1.37 ± 0.31 mag for the All sample. (The last value is not simply a weighted mean of the first two because the functions for red and blue galaxies have different shapes.) Thus, the evolution of M_B^* for both red and blue galaxies appears to have been very similar since $z = 1$.

Based on DEEP2 alone, we wondered in Paper I whether M_B^* for red galaxies in fact evolved very much, and indeed the slope derived from DEEP2 (black squares in Figure 7) is rather shallow. However, adding the points from COMBO-17 has steepened the slope for the high-redshift data, and this is bolstered by the addition of the local values from SDSS and 2dF. We return to this topic in §5 when discussing uncertainties in the red fits.

The bottom row of Figure 7 shows evolution in ϕ^* for the three color classes. Agreement is again very good among the data sets, but now red and blue galaxies evolve quite differently. The number density of blue galaxies remains nearly flat to $z = 1$, whereas the number density of red galaxies appears smaller back in time. This rise, already noted in connection with Figure 6, repeats very closely the pattern found by B04, whose data showed a gradual rise in ϕ^* since $z \sim 0.8$ by a factor of ~ 2 , preceded by a steeper rise before that near $z = 1$. The new data from DEEP2, which are completely independent, also show a steep rise near $z = 1$ followed by a shallower rise after that.

Formal values can be calculated for the decline in ϕ^* at $z = 0.8$ and at $z = 1$ using the new DEEP2 and COMBO-17 data together with the updated values of local ϕ^* shown in Figure 7. The mean value of ϕ^* at $z = 1$ is found to be $0.95 \times 10^{-3} \pm 14\%$, where the value comes from interpolating the DEEP2 and COMBO-17 data at $z = 0.9$ and $z = 1.1$ in Table 4 and the error reflects an assumed uncertainty of 20% in DEEP2 and COMBO-17 separately. The local value of ϕ^* is taken to be $3.44 \times 10^{-3} \pm 20\%$, where the error is a conservative estimate for the mean of the two measured values in Figure 7. The formal value for the rise in red ϕ^* from $z = 1$ to now is therefore $3.6 \pm 24\%$ (0.56 ± 0.09 dex), and the rise since $z = 0.8$ is $2.3 \pm 24\%$ (0.36 ± 0.09 dex). These are formal values based on the fitted values for ϕ^* ; potential errors and uncertainties are discussed in §5.

The fall in the number of red galaxies back in time measured here does not agree with the earlier result from

DEEP1 by Im et al. (2002) in which ϕ^* for red galaxies was claimed to have held constant since $z \sim 1$. The two redshift bins from Im et al. are plotted as crosses in Figure 7, where they lie both low and remain constant back in time. Im et al. applied a very stringent cut to define their sample, targeting only morphologically normal, spheroid-dominated E/S0s having red colors that are consistent with passively fading stellar populations. Their numbers therefore have to be corrected upwards in any event by $\sim 30\%$ to account for non-E/S0 contamination on the distant red sequence (Bell et al. 2004a, Weiner et al. 2005). However, the real difference between Im et al. and DEEP2 is nearly a factor of two, based on counts by DEEP2 over the identical region. The reason for this bigger discrepancy has not yet been unravelled and signals that the cut used by Im et al. to define their sample was even more stringent than thought. Finally, Im et al. compared their distant values to an earlier estimate for the local number density of spheroidal galaxies that is considerably lower than the values used here. When all of these factors are combined (and coupled with a new and somewhat larger cosmic variance estimate), it is easy to see why Im et al. reached the conclusion they did. However, this case highlights the problems introduced by selecting distant red galaxy samples in different ways, to which we return later below.

Before leaving Schechter fits, we report a further test that divided the DEEP2 and COMBO-17 blue samples into two equal halves to see whether “Moderately Blue” galaxies evolve differently from “Very Blue” galaxies. This repeats a test reported in Paper I for DEEP2 but now adds COMBO-17. The method of division used sloping lines that ran parallel to the red-sequence color-magnitude relation and bisected the blue sample in each redshift bin into equal color halves. The lines used for DEEP2 are illustrated in Figure 4 of Paper I; those for COMBO-17 were similar. Dynamically adjusted zero points for each redshift bin were used in preference to a constant color zeropoint because the latter would yield a spurious evolution if blue galaxies were reddening with time, as suggested by the motion of the median dividing line by ~ 0.1 mag for DEEP2 in Paper I. With this approach, M_B^* for Moderately Blue galaxies in DEEP2 was found to average 0.7 mag brighter than for Very Blue galaxies, as expected from the sloping color-magnitude relation for blue galaxies. Apart from that, the two blue sub-samples evolve similarly, with ϕ^* holding constant for both halves separately and values of M_B^* retaining a constant offset versus redshift. COMBO-17 confirms these conclusions. This sameness of evolution is perhaps surprising—we might have expected Moderately Blue galaxies to evolve in a way that is intermediate between Very Blue and Red galaxies. Work in progress shows, for example, that the clustering of Moderately Blue galaxies is indeed intermediate between the outermost color classes (A. Coil et al., in prep.). To the contrary, the data suggest that blue galaxies are evolving *as a bloc* in the CM diagram (apart from a possible dilation or expansion in their total color range, which cannot be tested in the present data).

We end this section by comparing to other published luminosity functions divided by color classes. The discovery of color bimodality is rather recent, and the study by Giallongo et al. (2005) is one of only two that divide dis-

tant galaxies by restframe color as we do. Unfortunately, a quantitative comparison cannot be given because no results were presented for epoch $z \sim 1$ specifically, and our data do not go farther than that. Plots in Giallongo et al. agree with ours in showing similar dimming for both red and blue galaxies, a constant number of blue galaxies, and a rise in the number of red galaxies since $z = 1$. Though the Giallongo et al. sample is much smaller than ours, it goes roughly two magnitudes fainter and is therefore valuable for establishing the existence of a *turnover* in the faint red luminosity function at $z \sim 1$.

A similar turnover is seen in the second study, by Cross et al. (2004), who counted red-selected galaxies and galaxies morphologically selected to be spheroids regardless of color, based on ACS images. Their counts agree well with ours despite their small sample size of 72 galaxies. The main difference with us is an even steeper turnover in faint-end slope near $z \sim 1$ in their red-selected sample, for which they find $\alpha \sim +0.3$; this is reduced to $\alpha \sim -0.5$ when blue spheroids are included.

Several other studies have attempted to count galaxies in various ways to see whether spheroids are disappearing back in time. Reviews can be found in Schade et al. (1999) and Im et al. (2001). Motivated by predictions of semi-analytic models, Kauffmann et al. (1996) reanalyzed CFRS data and claimed a drop in spheroid density, but their conclusions were disputed (Totani & Yoshii 1998). Schade et al. (1999) and Menanteau et al. (1999) counted morphologically normal $R^{1/4}$ -law objects in HST images out to $z \sim 1$ and concluded that there was indeed no drop. Sample and field sizes were small in both cases and no color cuts were applied, with the result that half or more of all distant objects were blue. Thus, there is no contradiction with the present study though the prevalence (again) of blue spheroids raises interesting questions. We return to the topic of blue spheroids in the Discussion section.

Our final reference is to CFRS, the pioneering study that first attempted to calculate the luminosity functions of distant red and blue galaxies separately (Lilly et al. 1995b). For blue galaxies, CFRS claimed a steepening in total faint-end slope back in time to $z = 1$. As noted, we have refrained from drawing any strong conclusions about faint-end slope evolution from our data, despite the fact that DEEP2 and COMBO-17 have many more galaxies and go 1.5 magnitudes deeper than CFRS. In retrospect, the CFRS data do not look strong enough to support that claim. For red galaxies, CFRS found no evolution in either M_B^* or ϕ^* , whereas we find a dimming of M_B^* by $\gtrsim 1$ mag and a rise in ϕ^* by a factor of ~ 4 (since $z = 1$). Part of the difference may be that, lacking knowledge of color bimodality, CFRS used a non-evolving color cut that did not quite hit the valley at high redshift. Regardless, CFRS projected a picture in which red galaxies have been rather static since $z = 1$, while blue galaxies have significantly changed. The picture derived in this paper is that blue galaxies are rather constant in number (though fading) over this time interval, while red galaxies are actively being generated. The general impression in CFRS of active blue galaxies versus passive red galaxies is thus essentially opposite to what we find.

4.3. Luminosity Density

Luminosity density provides an estimate of the total amount of light emitted by galaxies per unit volume. The luminosity density (in Johnson B band) in this work is obtained assuming the Schechter form of the luminosity function:

$$j_B = \int L\phi(L)dL = L^*\phi^*\Gamma(\alpha + 2), \quad (3)$$

where j_B is calculated in solar units using $M_{B\odot} = 5.48$ (Binney & Merrifield 1998) and Γ is the Gamma function. Use of this expression entails extrapolation over faint magnitudes that are not observed, the more so at high redshifts. However, fitting a given bright-end data set assuming different values of α tends to leave the product $L^*\phi^*$ unchanged, which means that most of the uncertainty comes from Γ . For example, changing α from -1.3 to -1.7 , as suggested by VVDS for their All sample at $z = 1.1$, changes Γ by 230%. This case is extreme, however. Values of α for Blue and All galaxies from nearly all other studies range between -1.0 and -1.3 , which implies a total change in Γ of only 30%. Plausible red α 's range in value from -0.5 to -1.0 , which changes j_B by only 11%. We conclude that, as long as α 's remain below -1.3 , uncertainties on j_B are small.

The resultant B -band luminosity densities are plotted versus redshift in Figure 8. To the previously shown local points we have added a second value for SDSS measured by Blanton et al. (2003). This latter value has been multiplied by 62% and 38% to obtain the fraction of B -band light in blue and red galaxies separately, based on fractional light contributions from Hogg et al. (2002).

Local values agree remarkably well for all three color classes. Relative to them, DEEP2, COMBO-17, and FDF show at most a mild decline in j_B for all galaxies with time. The fall in VVDS is nearly twice as large owing to their steeper faint-end slope at high redshift; however, as noted, FDF goes 10 times fainter and does not see such steepening. If constant α is adopted, as in DEEP2, COMBO-17, and FDF, the data indicate that j_B for all galaxies has fallen by about a factor of ~ 2 since $z = 1$. The CFRS survey (Lilly et al. 1996) is also plotted in Figure 8 and shows a much steeper decline in j_B after $z = 1$, like VVDS. Some of this may come from their steeper faint-end slope at high redshift, but part also comes from their adopted low local value (see figure), which they took from Loveday et al. (1992). The new value measured by 2dF and SDSS is about 30% higher.

Turning to the individual color classes, we see that the luminosity density of blue galaxies (in Figure 8b) as measured by DEEP2 and COMBO-17 evolves somewhat more than total luminosity density, falling by a factor of ~ 3 since $z = 1$. This is consistent with the constant value of ϕ^* and the change in M_B^* of 1.3 mag seen above for blue galaxies. Red galaxies are shown in Figure 8c, repeating a similar figure from B04. The conclusions are the same—the B -band luminosity density of red galaxies has remained essentially *flat* since $z = 0.9$ and was possibly rising before that. The flat section is caused by the dimming of M_B coupled with the rise in ϕ^* so that j_B remains constant. Before $z = 0.9$, the steep decline in ϕ^* wins out, and total j_B seems to be lower.

To summarize, DEEP2 agrees with both old and new

analyses of COMBO-17 in showing that the B -band luminosity density for red galaxies has remained nearly constant since $z = 0.9$, with a possible fall beyond that. Despite the fact that only the upper part of the function is observed at $z \sim 1$, DEEP2 and COMBO-17 agree within 20%, and extrapolation errors must be small because the red function is known to turn over, even at high redshift (Cross et al. 2004, Giallongo et al. 2005). Barring actual loss of galaxies from the samples (see below), the constancy of j_B for red galaxies after $z \sim 1$ should therefore be well established. Since stellar mass-to-light ratios are increasing with time (see below), this constancy implies that the stellar mass bound up in red galaxies has increased markedly since $z = 1$, as stressed by B04. Given the strong implications of this result for galaxy formation, it is advisable to go back and review the errors and assumptions, which we do in the next section. Readers not interested in these details should skip directly to §6.

5. ERRORS, ASSUMPTIONS, AND UNCERTAINTIES

This section focuses on red-sequence galaxies, although many of the conclusions apply equally well to the other color classes. A major issue is whether the apparent fall in the number density of bright red galaxies back in time is due to galaxies that are being left out in different stages of the analysis. A second issue is the extent to which the conclusions are sensitive to fitting the counts with Schechter functions having constant, non-evolving α . These effects and others are discussed below.

1) *Completeness of the photometric catalogues:* The COMBO-17 photometric catalogue has a $5\text{-}\sigma$ detection limit down to $R_{AB} \sim 26$, nearly two magnitudes below what is needed for the luminosity function surveys ($R_{AB} \sim 24$). The DEEP2 catalog is shallower but also adequate ($5\text{-}\sigma$ limit $R = 24.5$, Coil et al. 2004). DEEP2 makes an additional cut in surface brightness when designing the DEIMOS masks that deletes low-surface-brightness galaxies in the last half-magnitude bin (see Paper I). However, this is largely taken into account by calculating weights as a function of color as well as magnitude. Furthermore, this cut would not affect early-type galaxies, which have high surface brightness.

Errors in star-galaxy separation may result in either too few or too many galaxies, depending on the errors. Star-galaxy separation in COMBO-17 is based on 17-color photometry and is in general highly efficient; red counts near $z = 1$ may be $\sim 10\%$ too high owing to K-star interlopers (W04), but this would tend to *overestimate* red galaxies. Star-galaxy separation for DEEP2 was tested in Paper I using high-resolution HST images that cover part of the DEEP2 region in the Groth Survey Strip. Misclassification of red galaxies as stars amounted to $\sim 10\%$, but these were nearly cancelled by stars misclassified as galaxies, so the net effect was nil. Finally, checks of both data sets show that almost all galaxies to $R = 24$ have adequate photometry in all bands, and the few ($\sim 1\%$) DEEP2 galaxies that do not have B -band photometry (“ B -dropouts”) are corrected for statistically in the weights (Paper I).

2) *Dividing red galaxies from blue galaxies:* This is done using restframe values of $U - B$ in DEEP2 and $U - V$ in COMBO-17. Errors in the zero points of these systems do not matter even if they vary as a function of

redshift, since the dividing line is adjusted empirically to fit the color valley in each redshift bin. Division of local samples into red and blue galaxies has been done in different ways, but results are not sensitive to the method used. Madgwick et al. (2002) separated 2dF galaxies by spectral type, whereas Bell et al. (2003) separated SDSS galaxies based on concentration and optical color. Since there is very high correlation among these properties for local galaxies, it is not surprising that the results agree well, as shown in Table 5.

3) *Errors in M_B :* Weiner et al. (2005) checked DEEP2 restframe values of M_B against values derived from GIM2D photometry of Groth Strip HST images by Simard et al. (1999). GIM2D fitted model bulge+disk profiles to V and I images to find total magnitudes, whereas the DEEP2 Hawaii CFHT photometry approximates each object by a Gaussian profile on the BRI ground-based images. Despite these different methods plus uncertainties in HST WFPC2 photometric zero points and charge-transfer-efficiency corrections, the zero points of both M_B systems agreed to 0.07 mag. Furthermore, any mismatch in the magnitude systems for distant and local surveys would cause only an error in the evolution of M_B , not ϕ^* . The COMBO-17 luminosities have never been independently checked. However, the detailed SED information allows a precise calculation of the restframe B -band luminosity at all $z < 1$ without extrapolation. The main source of error is the photo- z error, which translates into a distance error. Most objects should have luminosity errors between 10% and 20%. Local survey values of M_B are claimed to be accurate to 0.1 to 0.02 mag (for photographic 2dF and CCD SDSS magnitudes respectively).

4) *R -band selection effect:* The use of the R -band for selecting DEEP2 and COMBO-17 corresponds to restframe 3300 \AA at $z = 1$, where the SEDs of red galaxies are rather dim. It might be thought that red galaxies are being “missed” on that account. In practice, this is completely allowed for by calculating limiting absolute magnitudes at each redshift as a function of both redshift *and* color using CM diagrams like those illustrated in Figure 4. The limiting M_B^* magnitude to which the counts are complete at each redshift and color is well understood.

5) *Redshift completeness and accuracy:* Redshift completeness has been simulated for COMBO-17 using Monte Carlo methods (W01, W03, W04). From these, it appears that redshifts are highly complete for red galaxies in COMBO-17 but substantially incomplete for blue galaxies in the last magnitude bin. This is consistent with the finding that nearly all failed galaxies are faint blue galaxies. Testing the completeness model independently is difficult. However, we have predicted total galaxy number counts from the best-fit luminosity functions, including extrapolations to the faint end and to somewhat higher redshifts, and find remarkable consistency of the prediction with the observed galaxy number counts in COMBO-17. Of course, the power of this test to assess the completeness of a sub-sample in any particular redshift bin is extremely limited.

Redshift incompleteness in DEEP2 was discussed in Paper I. Using the minimal versus the average model for failed redshifts typically results in no change in M_B and a change in ϕ^* of 10-20%, a small effect compared to

the total measured evolution in ϕ^* out to $z = 1$. Our preferred choice for red galaxies results in *higher* values of ϕ^* , which minimizes the observed evolution. For red galaxies, Paper I also considered a third, extreme model in which all failed red galaxies were assumed to be located in *whatever redshift bin was under consideration*. It is possible to do this without redshifts because red-sequence galaxies near $z = 0.7 - 1.1$ have apparent $R - I > 1.25$ and show up as a well defined ridge in the apparent CM diagram (see Figure 1 of Paper I). This test amounts to counting all possible red galaxies and dumping all of them with unknown redshifts into a *single* redshift bin. Even this extreme approach hardly affects results out to $z = 0.9$ (though it does increase both counts and j_B at $z = 1.1$).

Errors for DEEP2 redshifts used here are negligible ($< 10^{-4}$ in z); catastrophic errors are at the level of 1%. The accuracy of COMBO-17 photo- z 's has been studied using simulations, yielding an estimated rms error of 0.03, which agrees with the spectroscopic cross-check in W04. The effect of such errors on the red luminosity function was simulated by B04 and shown to be small.

6) *Formal Schechter fit errors and cosmic variance:* The errors in ϕ^* for red galaxies in Table 4 include Poisson noise and cosmic variance. In the two most distant bins, these errors are comparable and give an rms error in number density of about 20% per survey, or 14% for the two together. The error in the local zero point of ϕ^* for red galaxies is estimated to be 20%, yielding a formal rms error for the total difference between near and far samples of 24%, or 0.09 dex. This is small compared to the formal rise in ϕ^* since $z = 1.0$ of 3.6, or 0.56 dex.

This completes the list of possible observational errors and selection effects. We turn now to various theoretical and model assumptions.

7) *The assumption of a constant Schechter-function shape at all redshifts:* In practice, this means 1) that the Schechter formula is a good match to the bright end of the luminosity function, and 2) that the shape parameter α can be assumed to hold constant with redshift. A breakdown in either one of these assumptions will produce a mismatch between the data and the model, causing errors in both M_B and ϕ^* . If the shape of the real function is constant with redshift but is not well fitted by the model, the fitted parameters will drift with z as the data are limited to progressively brighter magnitudes at higher redshift. Any real evolution in shape may cause additional errors.

Inspection of Figure 6 suggests that our Schechter model (with the adopted value of $\alpha = -0.5$) *looks* like a good fit for red galaxies. Paper I tested this quantitatively by truncating DEEP2 data in nearer bins at brighter magnitudes corresponding to the cutoffs in more distant bins. For red galaxies, a drift of M_B^* of ~ 0.1 mag toward fainter values was seen with more truncation, whereas the measured evolution is a brightening of M_B^* by 1.3 back in time. The quantity ϕ^* drifted upwards by ~ 0.10 dex, whereas the measured evolution is a fall of 0.36 dex to $z = 0.8$ and 0.56 dex to $z = 1.0$. The measured evolutions are therefore if anything an *underestimate* owing to errors in assumed Schechter function shape. High-redshift bins cannot be tested in the same way, but visual inspection indicates that the match between data and model remains good.

However, certain recent data hint that the shape of the red luminosity function *may* be evolving with time, which would invalidate the assumption of strictly constant α . For example, de Lucia et al. (2004) see a deficit in the number of faint red galaxies in rich clusters at $z = 0.8$ compared to Coma, and Kodama et al. (2004) detect a similar deficit of faint red galaxies in overdense field regions at $z \sim 1$. As noted above, Cross et al. (2004) report a turnover in the counts of distant field red galaxies at $z \sim 1$ that is stronger than reported for red galaxies locally. These studies at high redshift all go 1-2 mag fainter than DEEP2 and COMBO-17 and are thus better determinants of α in distant samples. Added to this is the potential flattening of faint-end slope seen by COMBO-17 in its nearest redshift bin (see Figure 6), which resembles the flattish faint-end slope seen in local SDSS data by Bell et al. (2003) (though DEEP2 and 2DF [Madgwick et al. 2002] disagree; see Table 5).

A flatter faint-end slope with time might indicate that smaller red-sequence galaxies formed later than larger ones. Further support for this are findings by McIntosh et al. (2005) that smaller red-sequence galaxies evolve faster in surface brightness back in time than larger ones, by van der Wel et al. (2005) that the zero-point of the fundamental plane evolves faster back in time for small galaxies than for brighter ones, by Bundy et al. (2005) that the crossover mass between spheroids and disk galaxies was larger in the past, by Treu et al. (2005a,b) that small spheroidal galaxies arrived later on the red sequence than large ones, and by Im et al. (2001) and Cross et al. (2004) that distant blue spheroidal galaxies are significantly smaller than red ones and would preferentially populate the *bottom* end of the red sequence if they were fading towards it.

In short, recent data may be pointing toward a mild flattening in the faint-end slope of the luminosity function for red galaxies, with small spheroidal galaxies forming later than large ones. However, even if this is occurring, the effect on Schechter parameters is not large. Suppose for example that α is evolving from -0.5 at $z \sim 1$ to -1.0 locally, which is the largest change conceivably allowed by the data. Values for DEEP2 and COMBO-17 use $\alpha = -0.5$, while local surveys find the average value $\alpha = -0.65$ (Table 5). As an experiment, we have refitted local data using $\alpha = -1.0$,²⁰ and find that M_B^* brightens by 0.3 mag, ϕ^* declines by 0.18 dex, and j_B declines by 2%. These changes are all small compared to the claimed evolution. We also noted above that Γ itself varies by only 11% over the entire range $\alpha = -0.5$ to -1.0 . The conclusion is that faint-end slope is sufficiently flat for red galaxies that total luminosity density is determined quite well by data down to L^* , as is the case at all redshifts here.

8) *Using color as a surrogate for morphological type:* In focusing on red galaxies, we are implicitly assuming that restframe color is a good way of finding spheroidal-dominated E/S0 types at high redshifts. The method clearly works well at low redshifts, where only 15-20% of nearby red-sequence galaxies have Hubble types later than S0, being mostly edge-on and dust-reddened (Stratèva et al. 2001, Weiner et al. 2005). However, con-

²⁰ For example, using sample data available at <http://www.mpia-hd.mpg.de/homes/bell/data/glfearlycol.out>

tamination by non-spheroidal galaxies is larger at higher redshifts, amounting to 30% at $z \sim 0.75$ (Bell et al. 2004a, Weiner et al. 2005), and may increase beyond that (Cimatti et al. 2002a, 2003; Yan & Thompson 2003; Gilbank et al. 2003; Moustakas et al. 2004). Because contamination appears to be larger back in time, our measured rise in the number of red galaxies is a lower limit to the rise of *morphologically normal* E/S0s. Assuming that contamination on the red sequence at $z = 1$ amounts to 30% would increase the rise in normal E/S0s by 0.06 dex (to 0.62 dex) since that time. The true correction could be larger since contamination at $z = 1$ may be higher than at $z = 0.75$.

9) *Uncertainties in evolving stellar mass-to-light ratios:* These come into play when converting luminosity density into the more fundamental quantity stellar mass, as shown below. As noted, j_B for bright red galaxies above L_B^* is nearly constant out to $z = 0.9$, and may be lower before that. Since stellar mass-to-light ratios are increasing with time, this means that the stellar mass bound up in red-sequence galaxies must also increase. But by how much? B04 investigated this question using single-burst, passively evolving models, but these are only one option. We have investigated further possibilities such as τ models, “frosting” models with a continuing low level of star formation (e.g., Gebhardt et al. 2003), and “quenched” models in which star formation is shut down abruptly at some epoch (J. Harker et al., in prep.). Models are set up to match the average color of red-sequence galaxies today and the relatively small amount of color evolution that is seen since $z = 1$ ($\Delta(U - B) = 0.15 - 0.25$ mag; Bell et al. 2004b, Weiner et al. 2005, Koo et al. 2005). Recipes that satisfy these constraints all yield fading in M_B^* between 1 and 2 mag.

Observationally measured brightenings are consistent with these model estimates. The fundamental plane zeropoint brightens by 1-2 mag (van Dokkum et al. 2000, Gebhardt et al. 2003, van Dokkum & Ellis 2003, Treu et al. 2005a,b, van der Wel et al. 2005), the magnitude-radius zeropoint brightens by 1-1.6 mag (Trujillo & Aguerrí 2004; McIntosh et al. 2005), and M_B^* for red galaxies brightens by 1.3 mag (this paper). These observational shifts do not necessarily represent the fading of stellar populations if galaxies are merging or otherwise evolving in radius or σ and changing their structure. Nevertheless, it is striking that the amount of evolution from the various scaling laws is very close to the evolution seen in L_B^* , and this in turn is near the middle of the range predicted by the stellar population models. Combining all results together, we adopt 1.0 mag (0.4 dex) as the *minimum* increase in the mass-to-light ratio of a typical massive red galaxy since $z = 1$. Since luminosity density j_B has remained constant, this is also the minimum increase in red stellar mass over the same period.

We collect together the following potential corrections to the above estimates of $\Delta\phi^*$ for E/S0 galaxies from $z = 1$ to now. A positive sign means that the previously estimated rise in ϕ^* would be even bigger. The factors are: a possible mismatch between the adopted Schechter function shape and the actual bright end of the luminosity function, +0.10 dex; a possible nearby flattening of α from -0.5 to -1.0, -0.18 dex; and contamination by distant non-E/S0s, +0.06 dex. Each effect is small, two

of the three are hypothetical, and collectively they tend to cancel. For these reasons, we do not apply any corrections to the above-measured rise in ϕ^* , namely, 0.36 dex since $z = 0.8$ and 0.56 dex since $z = 1$.

We have not thus far uncovered any “smoking gun” as to why our counts of red galaxies in DEEP2 or COMBO-17 should be seriously in error. Nevertheless, there is a worrisome feature of the data, and that is the fact that the two surveys, DEEP2 and COMBO-17, do not show much *internal* evolution in ϕ^* over most of their well-measured range. This point was mentioned in Paper I in connection with DEEP2, and it is visible again in Figure 7, which plots both DEEP2 and COMBO-17. In both data sets, there is a jump in ϕ^* of ~ 0.2 dex from the distant surveys to the local surveys, and another jump of ~ 0.3 dex between $z = 0.9$ and $z = 1.1$. In between, ϕ^* tends to plateau. This stagnation is illustrated another way in Figure 9, which overplots $1/V_{max}$ data points from the lowest bin at $z = 0.3$ from both surveys on top of the data points for distant bins. As previously noted, the red counts at bright magnitudes tend to translate *parallel* to themselves, and one might even conclude that *no evolution* in the luminosity function, and thus in number density, has occurred. Both DEEP2 and COMBO-17 are similar in this regard. This degeneracy could be broken by having fainter data, but our two surveys do not go deep enough to permit this.

At this point, the argument involving stellar mass-to-light-ratios assumes great importance. Imagine replotting Figure 9 versus *stellar mass* instead of M_B . To account for the evolution in mass-to-light ratio, based on the discussion immediately above, the counts at $z \sim 1$ would have to be shifted over to the right by at least 1 mag, which would produce a vertical offset with respect to the low-redshift counts by about a factor of four (0.6 dex) near $M_B = -22$, where all curves superimpose. This is nearly identical to our previously measured fall-off of 0.56 dex based on ϕ^* . Thus, once mass-to-light ratio evolution is allowed for, the number of massive red galaxies *at fixed stellar mass* is increasing about as fast as the formal fit for ϕ^* . This argument is very similar to the one applied by B04 to *total* luminosity density, but we apply it here to individual galaxy masses at the top end of the luminosity function. The distinction is a small one, but we wish to emphasize that the present version of the argument relies entirely on data that are observed.

In summary, the conclusion that the number density of red galaxies has risen significantly is supported by three pieces of evidence. One is the fitted results for ϕ^* , which yield formally significant values in number density that agree very well between DEEP2 and COMBO-17. However, these may be suspect because of difficulties in comparing to local surveys and because both surveys may be prone to unknown errors at the far edge of their range. The next two arguments are therefore important and rest on the high probability that stellar mass-to-light ratios of red-sequence galaxies have evolved by at least one magnitude since $z = 1$. If so, the constancy of total luminosity density j_B implies a rise in total red stellar mass by the same factor. Finally, the constancy of the luminosity function itself (at the bright end) implies that a comparable growth in the number of massive red galaxies (at fixed stellar mass) must also have occurred. In what follows, we adopt the formal values of ϕ^* ($\Delta\phi^* = 0.36 \pm 0.09$

dex since $z = 0.8$ and 0.56 ± 0.09 dex since $z = 1.0$) as our measures of the rise in the number of red-sequence galaxies.

6. DISCUSSION

6.1. A “Mixed” Scenario for the Formation of Spheroidal Galaxies

The most interesting conclusion to emerge so far from the study of luminosity functions since $z = 1$ is the growth in red galaxies *over recent times*. We have argued that this translates to a similar, or even steeper, rise in the number of morphologically normal, spheroid-dominated E/S0s. Barring mergers among a large and undiscovered population—which would have to be tiny and/or highly obscured to avoid detection in our and other surveys—this discovery means that the immediate precursors of most massive E/S0s *must be visible in existing samples* at $z = 1$ and below. The implications of this were discussed by B04. We build on their arguments by adding data on the Blue luminosity function (measured here by DEEP2 and COMBO-17) and the properties of local spheroidal galaxies, which we will argue also have strong implications for formation scenarios. Our discussion focuses on *typical* red galaxies at high redshift since DEEP2 and COMBO-17 sample all galaxies regardless of location. The red sequence in distant clusters has also been extensively studied, but in general we do not try to fold these data into the present picture at this time.

It is well established that residence on the red sequence requires that the star formation rate be quenched, or at least strongly reduced. Stellar populations become red enough to join the red sequence just 1-2 Gyr after star formation is stopped (J. Harker et al., in prep.), but, in order for them to stay there, the star formation rate must remain low. For example, Gebhardt et al. (2003) explored a “frosting model” with an early high rate of star formation, followed by a slowly decaying τ component. Based on colors, they found that only 7% of total stellar mass could be formed in the τ component; more recent limits based on O II in distant red galaxies are even lower (N. Konidaris et al., in prep.). In short, as B04 pointed out, the large build-up seen in red stellar mass after $z = 1$ could not have arisen from star formation within red galaxies themselves. Rather, the stellar mass at the bright end of the red sequence must have *migrated* there via one of three processes: 1) the quenching of blue galaxies, 2) the merging of less-luminous already-quenched red galaxies, or 3) some combination of the two. In the following discussion, we focus on the *bright* end of the red sequence because this is where the data are complete. Galaxies may of course also be migrating to the lower end of the red sequence as well.

It is helpful to visualize this mass migration as the movement of progenitor galaxies through the color-magnitude diagram or, more fundamentally, the color-mass diagram. Sample tracks are shown in Figure 10. Two parent regions are illustrated, a narrow red locus corresponding to the red sequence, and a broader blue clump, which we will call the “blue cloud.” The rather constant morphology of the color-magnitude diagram since $z = 1$ suggests that these parent regions are relatively stable in size and location. In reality, they are also moving as galaxies evolve, but this will not be too important if individual galaxies move through them

more rapidly. With this assumption, we show the clumps as fixed and the galaxies as moving through them with time.

Each final galaxy today is represented by its most massive progenitor at any epoch. Stellar mass is migrating toward the upper left corner, where luminous red galaxies reside. For a galaxy to get there, two things must happen: the stellar mass composing the final galaxy must be assembled via gravitational collapse, and star formation must be quenched. A key question in the formation of red-sequence galaxies is therefore *when mass assembly occurred relative to star-formation quenching*: that is, did quenching occur early in the process of mass build-up, midway, or late? If extremely early, the pieces that would become the final galaxy migrated to the red sequence while still small, producing a large number of small galaxies on the lower red sequence that must later merge along the sequence in a series of “dry,” purely stellar mergers. This is Track A. If extremely late, the progenitors grew in mass hierarchically while still making stars within the blue cloud. Upon quenching, the most massive of them moved to the head of the red sequence and took up residence there without any further dry mergers whatsoever. This late-stage quenching scenario (for various masses) is shown as the tracks labeled B in Figure 10. Mixed scenarios are also possible, involving moderate mass assembly during the star-forming stage, followed by quenching and continued but limited dry merging along the red sequence. These are the tracks labeled C.²¹

The tracks in Figure 10 assume that quenching is accompanied (and perhaps triggered) by a major merger. A related but different scenario would involve the pure fading of *single* blue galaxies without any merging at all. We do not consider this, for two reasons given by B04. First, distant blue galaxies are disk-dominated (Bell et al. 2004b, Weiner et al. 2005), and fading alone cannot transform disks into spheroids—changing the structural morphology requires a merger. Second, there do not seem to be enough blue galaxies in the distant color-magnitude diagram with masses comparable to those of massive red galaxies (B04; Weiner et al. 2005; Paper I). Hence, in order to boost mass and to create spheroids, a final episode involving both quenching *and* merging seems to be required, at least for galaxies on the upper red sequence. On the other hand, quenching of pure disks without merging may well feed the *lower* red sequence. Indeed, the local red sequence contains many low-luminosity S0s (Binggeli et al. 1988) whose disks were probably quenched by ram-pressure stripping or other gas-starvation processes not involving merging.²² Because our focus here is on *massive* red galaxies, which

²¹ Strictly speaking, purely stellar mergers increase the stellar mass of a galaxy but leave its color unchanged. The arrows for an instantaneous merger should therefore be horizontal in Figure 10, which could add objectionably to the scatter on the red sequence if much merging occurred (Bower et al. 1992). On the other hand, the total merging process might last some time, in which case populations would age and redden as they grow in mass, causing the track to be tilted upward, which is how we have drawn it in Figure 10. Evidently, the total scatter induced by stellar merging depends on the precise timing and amount of merging. We return to this question in §6.3.

²² The red “thick-disks” of nearby spiral galaxies may be yet other examples of quenching without merging. A more likely explanation is that they are old-disk stars that have been dynamically

lack disks, a final episode of quenching plus merging is assumed.

Yet a third process by which galaxies might migrate to the red sequence is *unveiling*, whereby a dusty starburst is cleansed of its interstellar medium and the underlying galaxy is revealed. Such a process might cause the galaxy to brighten as dust absorption is removed, but also to redden as the starburst ages. However, there is no need to discuss this case separately because it is already subsumed under the above cases. If the starburst is an episode in the life of a single disk galaxy (e.g., Hammer et al. 2005), then the object today is a late-type spiral and is irrelevant to the red sequence. If the starburst has been induced by a merger, then the dusty phase is a temporary stage between the original blue precursor and the final red remnant, which does not alter our fundamental model of blue galaxies merging and turning into red galaxies. The arrows in Figure 10 are meant to connect initial and final states, not represent the detailed track whereby an object moves from blue to red. The only assumption that we have made concerning that transition is that merger remnants move quickly to the red sequence without lingering very long as bright blue starbursts. This is required by the fact that few if any bright blue starbursts are visible in the CM diagram (Bell et al. 2004b; Weiner et al. 2005; Paper I). It is also supported by radiative transfer models of dust in merging galaxies, which indicate that the burst itself is heavily cloaked by dust and is optically nearly invisible (Jonsson et al. 2005). Thus, starbursting galaxies are hard to tell optically from non-starbursting galaxies, and both types populate the blue cloud, as we assume.

The above assembly processes could be represented equally well by tracks in the color-magnitude diagram as in the color-mass diagram, and the former would be closer to existing data. However, mass is the more fundamental parameter, its behavior under merging is easier to predict than light (because dust and starbursts are not a problem), and mass estimates for samples of distant galaxies are growing and soon will be a standard tool (e.g., Drory et al. 2004, Fontana et al. 2004, Drory et al. 2005, Bundy et al. 2005). With mass as the size variable, the motions of galaxies moving onto the red sequence are described by vectors moving both upward (redder) and to the left (more massive). The slopes of the vectors in Figure 10 correspond to equal-mass mergers (i.e., mass doubling); unequal mergers would have more vertical vectors.

Yet another perturbation to the model is the possibility that the most-massive progenitor might take up residence on the red sequence and then later merge with a smaller gas-rich galaxy. The resultant starburst could briefly move the remnant back to the blue cloud, followed by subsequent decay back onto the red sequence (e.g., Charlot & Silk 1994). However, such events (while they last) would create massive blue galaxies, which we have argued are rare. The events must therefore be short-lived and should not greatly distort our basic assumption that, once the most-massive progenitor galaxy enters the red sequence, the galaxy remains there permanently.

heated over time by encounters with molecular clouds, disk instabilities, and/or small satellite galaxies, in which case no quenching at all is needed to explain them.

We make three generic points before considering Tracks A, B, and C further. First, since the number of massive spheroidal galaxies (and their associated stellar mass) has been growing over time, the makeup of the population is not stable, and mean properties such as average color, stellar age, etc., are constantly being skewed by recent arrivals (the so-called “progenitor bias” phenomenon of van Dokkum & Franx (2001)). The population as a whole therefore cannot be modeled using classic, single-burst, monolithic-collapse models (e.g., Eggen, Lynden-Bell, & Sandage 1962, Larson 1975), even though certain properties, such as L_B^* and color evolution, seem to be well fit by such models—this similarity is a coincidence and these models must be abandoned. A related point pertains to what we mean by the “age” of a galaxy. In the monolithic picture, the age of spheroidal galaxies corresponds to the epoch at which the mass collapsed and the stars were formed (both were the same). In the new picture, each spheroidal galaxy has at least *three* characteristic ages—the epoch of major mass-assembly, the epoch of major star formation, and the epoch of quenching—all of which can be different.²³

The final point is the importance of *local* E/S0s in constraining formation models. Four local properties are relevant. The first is the basic fact that morphology correlates closely with average stellar age—disk stars are younger and blue, whereas spheroidal populations are older and red (e.g., Baade & Gaposchkin 1963). This fundamental datum motivates our basic assumption that the *same* process quenching star-formation also altered the morphology from disk-like to spheroidal. This process is believed to involve mergers with other similar-sized galaxies (Toomre & Toomre 1972; Toomre 1977; Mihos & Hernquist 1994, 1996; Barnes & Hernquist 1996). Many local merger remnants are known whose properties are consistent with their evolving into spheroidal galaxies once the acute merger phase is over (e.g., Schweizer 1982, Schweizer 1986, Hibbard 1995). The incidence of spheroid-dominated galaxies is also higher in groups and clusters of galaxies (e.g., Dressler 1980, Postman & Geller 1984, Hogg et al. 2003, Balogh et al. 2004, Baldry et al. 2004), where mergers were more frequent.

Second, local E/S0 galaxies populate a rather tight “fundamental plane” linking radius, luminosity, and velocity dispersion (Faber et al. 1987, Dressler et al. 1987, Djorgovski & Davis 1987). The tightness of this plane implies that stellar mass-to-light ratio cannot scatter by more than $\pm 15\%$ at any point on the plane. Two other relations, the color-magnitude relation (Faber 1973, Sandage & Visvanathan 1978, Bower, Lucey & Ellis 1992) and the Mg- σ relation (e.g., Bender, Burstein & Faber 1992, Bernardi et al. 1998, Colless et al. 1999, Worthey and Collobert 2003), are also quite narrow and further link the properties of stellar populations to those of their parent galaxies.

Third, the mean light-weighted stellar-population ages of local Es scatter widely, from over 10 Gyr down to just a few Gyr (e.g., Gonzalez 1993, Trager et al. 2000a, Jørgensen 1999, Terlevich & Forbes 2002), with most be-

²³ Our use of the word *age* here is not meant to obscure the fact that mass assembly and star formation are both prolonged processes, so that any particular “age” must be the mean of events that may have lasted billions of years.

ing younger than classic single-burst models would predict (11.4 Gyr if $z_{form} = 3$). This large number of young ages allows room for the late quenching that is required by the luminosity function data. On the other hand, there is at most a weak trend in stellar age with mass or σ along the red sequence (Trager et al. 2001, Terlevich & Forbes 2002, Bernardi et al. 2005), so that stellar ages and metallicities scatter substantially at every point on all three relations. To keep the relations tight, Worthey et al. (1995) posited that an *anti*-correlation must exist between age and metallicity at constant mass and/or σ , as later verified by Jørgensen (1999), Trager et al. (2000b), and Bernardi et al. (2005).

The fourth and final point is that nearby Es populate a *structure sequence*, in which small objects rotate strongly, are flattened by rotation, and have disk isophotes and steep central surface-brightness profiles, whereas massive objects rotate weakly, are flattened by anisotropic velocity dispersions, and have boxy isophotes and core-type central profiles (e.g., Davies et al. 1983, Bender, Burstein & Faber 1992, Faber et al. 1997). At the low-mass end, these properties connect smoothly with S0s and, through them, to the remainder of the Hubble sequence (Kormendy & Bender 1996). Several authors have suggested that this structure sequence can be explained broadly by assuming that small spheroidals were produced via mergers of gas-rich, “wet” progenitors, while more massive spheroidals were produced by progressively “dry,” purely stellar mergers of smaller spheroidals (e.g., Bender, Burstein & Faber 1992, Kormendy & Bender 1996, Faber et al. 1997). This scenario implies that the most massive of today’s spheroidals were created mainly by purely stellar mergers.

With these points as background, we return to the tracks in Figure 10. The early-quenching scenario (Track A) has most of its mass-assembly occurring in dry mergers along the red sequence. This can be ruled out on two grounds. First, to produce the large amount of stellar mass bound up in massive red-sequence galaxies would require a huge reservoir of small, faint galaxies on the lower red sequence. This excess is not detected at any redshift—the local red-sequence luminosity function is at most flat ($\alpha \sim -1.0$) and if anything turns over more steeply at higher redshifts (Cross et al., 2004, Kodama et al. 2004, Giallongo et al. 2005, Figure 6 here). The required reservoir of small red galaxies therefore does not exist. Second, building up massive red galaxies from purely dry mergers along the red sequence would yield stellar populations whose metallicities are uncorrelated with stellar age and whose ages and metallicities would converge to a single value at high masses after many mergers had occurred. This fails to match the fundamental plane, color-magnitude, and Mg- σ relations, which indicate that age and Z must be *anti*-correlated at each location, nor does it match the strong spread in age and Z that exists even among massive galaxies (Trager et al. 2001, Terlevich & Forbes 2002). (The upward tilt that we have placed on the arrow representing dry mergers on Track A reflects the probable increase in mean stellar age during dry merging, not an increase in mean metallicity.)

The late-quenching scenario (Track B) is extreme in the opposite sense of having *no* dry merging at all along the red sequence. In this picture, massive present-day spheroidals were formed via a single merger of two very

massive *gas-rich* progenitors. The main reason for ruling out this scenario is the structure sequence among local Es, which, as noted, implies that massive Es were formed by dry, gas-poor mergers. The signatures of such mergers are distinctive because the precursors are dynamically hot, yielding fuzzy tidal tails without sharp boundaries; many examples of such dry mergers can be seen in local catalogues (e.g., Arp 1966), so it is clear that they are occurring.

The mixed scenario (Track C) involves early mass assembly and star formation, followed by quenching and further (but limited) dry merging. This scenario seems most naturally to explain the properties of local E/S0s. For example, the final mergers making small spheroidals would be mostly gas-rich, while later mergers along the red sequence would be progressively more gas-poor, as required by the structure sequence. Furthermore, the break point between boxy and disk galaxies is an upper limit on the masses of blue galaxies that have migrated onto the red sequence recently. That break point today is in the range $M_B = -20$ to -21 , where boxy and disk galaxies coexist (Faber et al. 1997, Lauer et al. in progress). With mean spheroidal $\mathcal{M}/L_B \sim 6$ (from Gebhardt et al. 2003, adjusted to the B -band and $H_0 = 70$), this translates to stellar masses in the range $1\text{-}2 \times 10^{11} M_\odot$, or blue progenitor masses of $0.5\text{-}1 \times 10^{11} M_\odot$ for equal-mass mergers. These are at the upper end of blue masses today (Bell et al. 2003), as expected.

With one more quite natural assumption, the mixed scenario might even be able to explain the narrowness of the local Fundamental Plane, color-magnitude relation, and Mg- σ relations. Consider a selection of galaxies at a fixed mass today on the red sequence. In the mixed scenario, these galaxies will have arrived there via different routes—some will have been produced by recent gas-rich mergers of two blue galaxies, while others will have quenched earlier and evolved along the red sequence via dry mergers for a longer time. In general, however, we expect there to be a broad correlation between the mass of a spheroidal galaxy today and the mass of its latest blue progenitor, massive spheroidals tending to come from more massive blue galaxies, and vice versa.

This “memory” of progenitor mass then helps to shape the final metallicity of a galaxy via the mass-metallicity relation among star-forming galaxies. This relation is strong among nearby galaxies (Tremonti et al. 2004) and apparently extended well into the past to beyond $z = 1$ (Kobulnicky et al. 2003). If the amount of dry merging on the red sequence is limited, the original mass-metallicity relation of the progenitors will survive to form the *backbone* of the red-sequence scaling relations seen today. On the other hand, this backbone will be blurred by the different star-formation histories of galaxies—galaxies that quenched early from low-mass blue progenitors and grew later via dry mergers will have rather low metallicities (reflecting their small progenitors), but their average stellar age will be high (since multiple dry mergers take time). In contrast, galaxies that quenched late and arrived on the red sequence near their present mass will have higher metallicities (reflecting more massive progenitors), but their average stellar ages will be younger because they quenched recently. Thus, the *multiplicity of routes* that is inherent in the mixed scenario might help to account naturally for the *anti*-correlation

between age and metallicity that is needed to explain the scaling relations. However, the more dry merging that takes place along the red sequence, the more the underlying mass-metallicity correlation of the blue progenitors will be erased, to be replaced by age scatter. The amount of scatter in age and Z at fixed mass is therefore an indicator of the amount of dry merging that could have occurred, which might be determined through observations and modeling.

6.2. Quenching and Downsizing

This section briefly discusses quenching and the related concept of “downsizing.” To be effective, quenching requires the removal of essentially all cold gas within galaxies, and the prevention of any more falling in. The key question is what triggers quenching: why and when does it happen? Several processes are probably involved. We adopt as a starting point the standard view that mergers of gas-rich galaxies can trigger powerful starbursts (e.g., Mihos & Hernquist 1994, 1996; Sanders & Mirabel 1996). One major source of gas removal is therefore consumption of gas in the starburst itself. The burst also generates internal stellar-driven feedback that can remove and/or heat gas, such as photoionization, O-star winds, supernovae, and radiation-driven winds operating on dust (Murray, Quataert & Thompson 2005). An additional source of gas-heating is orbital energy injected during the merger, which can drive gas out in a galactic wind (Cox et al. 2005). Gas can also be removed by external processes such as ram-pressure stripping, tidal stripping, and “harassment” (Moore et al. 1996), which operate more effectively in the dense environments frequented by spheroidal galaxies.

Despite this abundance of potential gas-removal mechanisms, it has been suggested that these alone may not be adequate to keep spheroidal galaxies gas-free—the energy requirements seem too large, and gas in models continues to fall in, creating large numbers of massive blue galaxies that are not seen, especially at the centers of clusters (e.g., Benson et al. 2003). For example, to match the sharp turndown at high masses in the galaxy mass function, Kauffmann et al. (1999) found it necessary in semi-analytic models to truncate gas cooling arbitrarily in all halos above a circular velocity of $V_{\text{circ}} = 350 \text{ km s}^{-1}$. Similar ad hoc recipes are being tested in smaller halos in order to see if they can produce color bimodality (e.g., R. Somerville et al., in prep.). Considerable evidence, both theoretical and empirical, suggests that feedback from AGNs might be the missing trigger for quenching (e.g., Granato et al. 2004; Dekel & Birnboim 2005; Springel, Di Matteo & Hernquist 2005), which is plausible since spheroids are precisely those galaxies that possess massive black holes (Kormendy & Richstone 1995, Magorrian et al. 1998, Tremaine et al. 2002).

Properties of local spheroids may shed further light on quenching. A major clue, as mentioned, is that local galaxies scatter significantly in age at any location on the red sequence, which suggests that galaxies of the same mass have arrived there via different routes and different quenching histories. It is also observed that red galaxies *co-exist* with blue galaxies over more than one order of magnitude in total stellar mass—a cross-over point exists near $3 \times 10^{10} M_{\odot}$ where the numbers of red and blue galaxies are equal (Kauffmann et al. 2003a,b),

but the transition is gradual (Bell et al. 2003). Both of these facts suggest that the trigger for quenching is *not* simply total stellar mass or any variable closely related to it (such as luminosity or rotation speed) because any of those would produce a division in mass between spheroidals and non-spheroidals that is too abrupt. Rather, we seek one (or more) variables that are broadly related to total mass but with considerable scatter, and perhaps also having some relation to the presence and size of the central black hole, given the possible need for AGN feedback. A natural variable satisfying these requirements is *stellar spheroid mass*, which increases generally with total galaxy mass but scatters greatly with respect to it. Spheroid mass is also closely linked to the mass of the central black hole (Kormendy & Richstone 1995, Häring & Rix 2004), and thus perhaps its energy output. Finally, spheroid mass increases discontinuously during a major merger, and its rise over some threshold might be the specific trigger for quenching. This scenario would meet the requirements of Balogh et al. (2004), who concluded that the blue-to-red transition must be driven primarily by internal properties rather than by environment. But environment could play a smaller role and, through its variation from galaxy to galaxy, contribute to the scatter seen in stellar ages at each point on the scaling relations.

As a final topic, we consider the matter of “downsizing.” The basic concept of downsizing was introduced by Cowie et al. (1996) to explain their finding that actively star-forming galaxies at low redshift are smaller in mass than actively star-forming galaxies at high redshift, which suggested that star formation is stronger at late times in smaller galaxies than large ones. The essence of this idea was already latent in the literature. For example, it was known that early-type galaxies are more luminous and more massive than later-type galaxies (de Vaucouleurs 1977, Binggeli & Sandage 1985) and that their stellar populations are on average older (e.g., Tinsley 1968, Searle, Sargent & Bagnuolo 1973). Color and gas fraction were known to vary systematically along the Hubble sequence (de Vaucouleurs 1977; Roberts 1969), indicating progressively slower, less-efficient star formation in later Hubble types. Finally, the blue end of the Hubble sequence had been shown explicitly to be a mass sequence (van den Bergh 1976, de Vaucouleurs 1977), with low-mass Irr Is at the bottom having the smallest fraction of stars and the highest proportion of gas (Roberts 1969). All evidence together thus indicated (even then) that massive galaxies made most of their stars early, whereas small galaxies formed theirs relatively later. Recent analyses of the star-forming histories of both local galaxies from SDSS (Heavens et al. 2004) and distant galaxies from the Gemini Deep Deep survey (Juneau et al. 2005) have confirmed this basic picture.

Blumenthal et al. (1984) offered a reason for this mass-dependent sequence by suggesting that early-type galaxies arose from higher- σ galaxy-sized perturbations in a cold-dark-matter universe. Such perturbations would collapse first and start making stars early. Moreover, because of the non-white nature of the CDM power spectrum, high- σ perturbations of galaxy mass are embedded preferentially within larger high- σ perturbations (Bardeen et al. 1986), which causes them to merge more and eventually wind up in groups and clusters. The

accelerated growth of high- σ perturbations was demonstrated in early hydrodynamical simulations by Cen & Ostriker (1993), which showed the first galaxies collapsing at the intersections of filaments, forming stars rapidly, and assembling later into groups and clusters. They identified these early-forming objects with E/S0s.²⁴

The above concept of downsizing refers to the *mean epoch of star formation*, which was clearly earlier in massive galaxies than smaller ones. However, as noted, spheroidal galaxies have a second star-formation timescale, namely, that of *quenching*. These two timescales might vary differently with mass, thereby generating (in principle) two different kinds of downsizing (or even *upsizing*). When speaking of downsizing, it is important to clarify which timescale is meant.

The remainder of this discussion focuses on the down(or up)sizing of *quenching*, asking whether the typical entry mass onto the red sequence has increased or decreased with time. This amounts to asking whether it is easier (or harder) to keep galaxies of a given stellar mass free of cold gas at late epochs. Three factors suggest that keeping galaxies gas-free should get easier with time. First, gaseous infall generally declines with time in the Universe, and gas within galaxies gets converted to stars; both of these mean that there is less gas overall that needs to be removed or fended off. Second, galaxies cluster more and move more rapidly within clusters, both of which promote environmentally-driven gas-removal processes such as stripping and harassment. Third, parent dark-matter halos have higher dynamical temperatures and lower densities so that any leftover gas outside galaxies is hotter and less likely to cool.

The sum of these factors suggests that it is easier to keep galaxies of a given mass gas-free at late times. When this is coupled with the observed fact (not yet fully explained) that quenched galaxies are larger, we are led to hypothesize that the typical entry mass onto the red sequence may be *decreasing* with time, such that progressively smaller galaxies can find their way onto the red sequence at later epochs. We have already mentioned certain observations that point in this direction, including the deficit of small red-sequence galaxies at high redshift (Kodama et al. 2004, Cross et al., 2004, Giallongo et al. 2005) followed by possible later infill (e.g., Bell et al. 2003; COMBO-17 here), the late arrival

²⁴ It has sometimes been said in the recent literature that CDM predicts that massive galaxies form late and should therefore have younger stars, which is opposite to what the Hubble sequence actually shows. This remark demonstrates confusion between the formation of galaxies and their dark-matter halos. Massive halos indeed form late, but they are making clusters of galaxies today, not galaxies. Baryonic dissipation has reduced the collisional cross-sections of galaxies to the point that galaxies are merging much more slowly now than their parent dark-matter halos. Indeed, it is this reduced merging of galaxies at recent times that enables the overall number density of galaxies, $\phi^*(\text{All})$, to remain constant since $z = 1$, despite the fact that halos are continuing to merge. The larger point is that events on the scale of galaxies are becoming progressively more decoupled from events on the scale of halos, including the processes of star formation and baryonic mass assembly (see also Heavens et al. 2004). But the influence of parent halos (what is often termed “environment”) has not yet declined to zero even now. The halo occupation distribution (HOD) and related statistics (see review by Cooray & Sheth 2002) are emerging as powerful tools for unravelling the relationship between galaxies and their dark-matter halos, which is crucial to understanding galaxy formation.

of small spheroids on the fundamental plane (Treu et al. 2005a,b), the more rapid evolution back in time of the surface-brightness of smaller spheroids (McIntosh et al. 2005), the more rapid evolution back in time of the fundamental plane zeropoint for smaller galaxies (van der Wel et al. 2005), and the possible decrease with time in the crossover mass between spheroids and disk galaxies (Bundy et al. 2005). In aggregate, the evidence may be pointing to a downsizing of quenching, on top of the downsizing of star formation in galaxies as a whole.

6.3. Related Topics

The finding that the majority of spheroidal stellar mass was quenched only after $z = 1$ amounts to a paradigm shift with wide repercussions over a range of issues in galaxy formation. This section lists some important questions that are raised by the late-quenching picture.

First, does the increase of mass on the red sequence cause a problem for the observed mass budget of blue galaxies? No, because the increase in red stellar mass is small in absolute terms. Red-sequence galaxies today make up 20% of the total number of bright galaxies, and 40% of the total stellar mass (Hogg et al. 2002). If their stellar has roughly tripled since $z = 1$, it would have increased from 0.13 units to its present level of 0.40 units. If this increase came at the expense of blue galaxies, their stellar mass would have declined from 0.87 units to 0.60 units, a fall of only 0.16 dex that if translated to ϕ^* would be barely detectable in Figure 7. Thus, even this extreme scenario in which all new stellar mass in red galaxies came *entirely* from the pre-existing stellar mass of blue galaxies is probably consistent with the data. But it is more likely that much of the new red stellar mass was born via continuing star-formation in blues after $z = 1$, and also in final merger-generated starbursts. For example, it has been claimed that 50% of all star formation at $z = 1$ is occurring in intermediate-mass LIRGS, many of which are mergers and could be the precursors of spheroidal galaxies (Hammer et al. 2005 and references therein). Total stellar mass in all types of galaxies has also probably increased since $z = 1$, by between 1.4 and 2.0 (Fontana et al. 2004; Rudnick et al. 2003; Drory et al. 2005; but see also Bundy et al. 2005). Either of these increases would be large enough to maintain blue ϕ^* approximately constant if the new stellar mass were appropriately distributed over red and blue galaxies. Thus, the observed constancy of blue number density in the face of rising numbers of red galaxies does not seem to be a problem.

A second point is how galaxy mass functions are predicted to evolve if the present luminosity function data are correct. We have already noted that the measured evolution in M_B^* for red galaxies is similar to the predicted change in their stellar \mathcal{M}/L_B ratio. If these evolutions are identical, the characteristic mass \mathcal{M}^* for red galaxies has remained constant. The same rough equality probably also holds for blue galaxies. But, since red galaxies are more massive than blue ones, their rise in number density should cause the mass function to go up faster at higher masses, and thus the mass function should change shape. This does not appear to agree with published measurements, which show a more even rise over all masses (Drory et al. 2005), or perhaps even no rise at all (Bundy et al. 2005). On the other hand, exist-

ing mass functions are measured over small areas and are subject to large cosmic variance. Larger samples coming soon from DEEP2 (K. Bundy et al., in prep.) and VVDS may resolve this discrepancy.

A third issue is reconciling the rise in red-sequence galaxies with the rate of mergers needed to create them. Estimated merger rates for bright galaxies going back to $z \sim 1$ vary widely in the literature (see Lin et al. 2004 and references therein). Early merger rates from DEEP2 are based on optical pair counts, not morphologies, and are rather low: only 9% of L^* galaxies are estimated to have suffered a major merger since $z = 1.2$ (Lin et al. 2004); Bundy et al. (2004) obtain similar rates based on K-band pair counts. In the present scenario, merged galaxies are assumed to migrate rapidly to the red sequence. If red galaxies have tripled in number since $z = 1$ and make up 20% of all galaxies today (Hogg et al. 2002), then 2/3 of all red ones—and thus 13% of all galaxies—must have merged since $z = 1$. This fraction 13% is not far from the DEEP2 merger fraction of 9%, and also does not allow for additional quenching that may have occurred without mergers, such as in stripped S0s. In short, the required rate of conversion by mergers is not excessive and may even be consistent with the rather low DEEP2 rate. Higher merger rates could also be accommodated provided that the extra remnants wind up as the bulges of spiral galaxies, as is generally assumed in semi-analytic models (Kauffmann et al. 1996, Baugh, Cole & Frenk 1996, Somerville & Primack 2001) and suggested by Hammer et al. (2005) based on the observed frequency of LIRGs.

A further puzzle that may now need rethinking is the existence of non-solar abundance ratios in early-type galaxies, which display enhanced ratios of SNe Type II elements compared to elements generated in Type Ia's (e.g., Worthey et al. 1992). The amount of enhancement correlates closely with velocity dispersion (Kuntschner 1998, Trager et al. 2000b). It has been customary to account for these non-solar ratios by appealing to very rapid star formation, which suppresses the iron-peak elements that are produced more slowly by Type Ia's. Such early-burst scenarios were natural within the monolithic-collapse picture. However, if most massive ellipticals were quenched at or after $z = 1$, they were probably making stars for at least several Gyr before that, and rapid-burst models may no longer apply. Perhaps a correlation existed among the *precursors* of red galaxies between σ and average star-formation duration that is strong enough to explain the data. Alternatively, other factors such as galactic wind strength or IMF variations (see Trager et al. 2000b) might play a role.

Finally, further work is needed to understand the form and scatter of the fundamental plane, Mg- σ relation, and red-sequence (color-magnitude) scaling relations. As noted, scatter about these relations places strong limits on the amount of stellar merging, which may prove problematic. The tilt of the red sequence is also a mystery: it could come from the underlying mass-metallicity relation of the blue progenitors or from aging during a long series of stellar mergers—both possibilities have been mentioned here. In short, the scaling relations are sensitive diagnostics. We might have attempted simple estimates of their form and scatter here, but semi-analytic models seem a much better vehicle for such calculations, and we

defer these to later papers.

Besides posing difficult questions, the late-quenching picture also opens up new opportunities. If red galaxies indeed emerged recently, it becomes feasible to study in detail why certain galaxies turn red. For example, we can look at the galaxy population just beyond $z = 1$ and try to predict which galaxies are about to be quenched. Given the close correspondence between red galaxies and dense environments, it is natural to ask whether galaxies turn red owing to an increase in the amount of clustering around them, or whether pre-existing dense environments suddenly begin to “spawn” red galaxies near $z = 1$. Two studies within DEEP2 are underway to answer this question (B. Gerke et al., in prep.; M. Cooper et al., in prep.), both taking advantage of DEEP2's high redshift accuracy, which provides the needed information on parent groups and clusters.

An important issue going well beyond the confines of this paper is the impact that the late-quenching picture will have on the relation between spheroids and black holes. The masses of present-day black holes correlate closely with the properties of their parent spheroids, whether with total luminosity (Kormendy & Richstone 1995, Häring & Rix 2004) or with velocity dispersion (Gebhardt et al. 2000, Ferrarese & Merritt 2000). As long as spheroids were thought to form early, it was possible to imagine that the relationship is ancient, with roots going back to $z \sim 2$ when spheroids and black holes were simultaneously forming (e.g., Richstone et al. 1998). However, if most spheroids emerged late, the relation could hardly have existed before $z \sim 1$, and the massive black holes that were growing before that time must somehow have “known” which spheroids they would eventually wind up in. Thus, the late-emergence of spheroids adds an important new twist to the black-hole/galaxy co-evolution story.

Although we have clearly come down in favor of the late-quenching picture, the conclusion is more indirect than we would like, resting heavily as it does on models for the evolution of stellar mass-to-light ratios. The subject would be on much firmer footing if further checks could be carried out. For example, it remains to be shown whether K -band counts and redshift distributions of near-IR-selected samples are consistent with the large drop in red galaxies at $z \sim 1$ claimed here. These counts should be reconsidered using fainter samples with photometric redshifts, and quenched rather than monolithic-collapse models. Furthermore, if the red counts could be extended just 1.5 magnitudes fainter, ϕ^* could be measured directly at $z = 1$. For definitive results, however, such data would have to cover $\sim 2 \square^\circ$ spaced over the sky in several statistically uncorrelated regions.

A related question is whether the emergence of spheroidal galaxies near $z = 1$ is consistent with the properties of red objects earlier than this. Some studies have searched for red objects beyond $z = 2$ (e.g., van Dokkum, et al. 2003; Franx et al. 2003), while others have targeted red objects near $z = 1.5$ (e.g., Cimatti 2002a). The results are very different. Objects beyond $z = 2$ contain old stars but are still star-forming vigorously; they are red in part because they are dusty (Förster Schreiber et al. 2004; van Dokkum et al. 2004; Toft 2005). Although they may be future red-sequence galaxies, their numbers do not bear on the question of

whether many galaxies quenched later near $z = 1$.

In contrast, the number of red galaxies near $z = 1.5$ is very relevant. Despite the fact that a large fraction of these objects are also dusty (e.g., Moustakas et al. 2004), a sizeable fraction also seem to be fully quenched (Longhetti et al. 2005, Daddi et al. 2005, Saracco et al. 2005). Number densities have been variously estimated between 10% (Daddi et al. 2005) and 100% (Saracco et al. 2005) of local massive spheroidals, leading different authors to conclude that massive Es are, or are not, fully quenched by $z = 1$. However, such surveys are as yet small and are subject to large cosmic variance. Extending this work to larger areas (and distinguishing dusty galaxies from quenched ones) would provide the sharpest test of the late-quenching model.

7. SUMMARY

The evolution of B -band galaxy luminosity functions since $z \sim 1$ is determined using a total sample of 39,000 galaxies to $R \sim 24$ mag from the DEEP2 and COMBO-17 surveys. DEEP2 data come from Willmer et al. (2005, Paper I), while the COMBO-17 data come originally from Wolf et al. (2003) but have been substantially reworked using improved photo- z 's and new color classes. Evolution is examined for blue and red samples separately by dividing galaxies using color bimodality; this is the first study aside from Willmer (2005) to compare blue and red galaxies in this way. Cosmic variance is reduced to 7-15% per redshift bin by combining the results of the surveys. DEEP2 counts agree remarkably well with COMBO-17 in all color classes at nearly all redshifts.

Luminosity functions of blue and red galaxies evolve differently with redshift; the blue counts shift to brighter magnitudes at fixed number density back in time, whereas red counts are nearly constant at fixed absolute magnitude. Both DEEP2 and COMBO-17 agree in this regard. Schechter function parameters are fit to the data assuming non-changing shape (constant α), and results are compared to recent measurements from other distant surveys. Good agreement is found between DEEP2 and COMBO-17 at all redshifts, and between these and other large, recent surveys counting all galaxies. Results by color are not yet available from these other surveys.

Combining the distant Schechter parameters with local ones, we solve for the fading over time of characteristic luminosity M_B^* for All, Red, and Blue galaxies. All classes fade by nearly the same amount, showing fadings (per unit redshift) of 1.30 ± 0.20 mag for red galaxies, 1.31 ± 0.14 mag for blue galaxies, and 1.37 ± 0.31 mag for all galaxies. In contrast to M_B^* , ϕ^* evolves differently in different color classes: formal values for ϕ^* hold steady for blue galaxies but rise for red galaxies by $0.36 \text{ dex} \pm 0.09 \text{ dex}$ since $z = 0.8$, and by $0.56 \pm 0.09 \text{ dex}$ since $z = 1$. The evolution of luminosity density, j_B , also differs with color; for blue galaxies it falls by 0.4 dex after $z \sim 1$, while for red galaxies it remains constant since $z = 0.9$, possibly being smaller before that.

The simplest interpretation of these results is that the number density of blue galaxies has remained nearly constant since $z = 1$, whereas the number density of red galaxies has increased. The latter conclusion is subjected to close scrutiny, which is warranted by the fact that *most* of the total red evolution (in both DEEP2 and COMBO-

17) occurs between the local surveys and our data, and in the farthest bin of our data—i.e., in the two places where the data are weakest. Although it is possible that our formal values of ϕ^* may have unknown errors, we nevertheless conclude that substantial evolution in the number density of red galaxies *has* occurred, based on strong evidence for a rise of at least one magnitude in the mass-to-light ratios (\mathcal{M}/L_B) of red stellar populations since $z = 1$. When this rise is taken into account, the observed near-constancy of red luminosity density translates to a rise in overall number density by at least one magnitude. A similar argument applied to the red counts at fixed absolute magnitude translates to a rise in number *at fixed stellar mass* that is also comparable to the formal rise from ϕ^* . Thus, both the new DEEP2 data and the reanalysis of COMBO-17 together strongly support the rise in red galaxies since $z \sim 1$ first found in COMBO-17 by Bell et al. (2004b). The rise in morphologically pure E/S0s is even larger if increasing contamination by non-E/S0s at higher redshifts is allowed for.

The implications of this rise for galaxy formation are examined. Barring the existence of a major, highly obscured and as-yet-unknown population of galaxies at low redshifts, the immediate precursors of most modern-day E/S0 galaxies must be visible in existing surveys near $z = 1$. The lateness of the rise is inconsistent with classic, high-redshift single-burst collapse models for E/S0 formation, which predict constant numbers of spheroidal galaxies over this epoch. Instead, it appears that most present-day E/S0s arose from blue galaxies with ongoing star formation that were “quenched” at or after $z \sim 1$ and then migrated to the red sequence. The properties of nearby E/S0 galaxies support a “mixed” scenario in which quenched galaxies enter the red sequence over a wide range of masses via “wet,” gas-rich mergers, followed by a limited number of “dry,” stellar mergers along the sequence. The most massive E/S0s are built up during the last stages of dry merging and are visible today as boxy, core-dominated ellipticals.

Some evidence points to a decline in the average entry-mass onto the red sequence with time, which would amount to a “downsizing” of quenching. This and other processes might change the shape of the red luminosity function, violating our assumption throughout of constant α , but the changes are not large enough to invalidate our major conclusions. Furthermore, galaxies at a given mass on the red sequence will have arrived there via different merging and star-formation histories. Plausible differences among these histories may account for the *anti*-correlation that is seen between age and metallicity residuals on the red sequence and that is needed to account for the narrowness of the fundamental plane, Mg- σ , and color-magnitude relations of local E/S0s.

Finally, growing evidence seems to suggest that extra feedback from AGN activity might be a key ingredient in initiating quenching. Consistent with this is the fact that quenched stellar populations and massive central black holes are both uniquely associated with spheroidal galaxies. We speculate that the specific trigger for quenching occurs when the spheroid stellar mass, and perhaps also the black-hole mass, exceeds a threshold value during a merger.

CNAW thanks G. Galaz, S. Rauzy, M. A. Hendry and K. D’Mellow for extensive discussions on the measurement of the luminosity function; E. Bell, J. Brinchmann, A. Gabasch, and G. Galaz for providing electronic versions of their data; S. Lilly for correspondence on the CFRS luminosity function, and G. Blumenthal, J. Cohen, and L. Cowie for useful discussions. SMF thanks R. Somerville, J. Primack, and T. Lauer for extensive discussions concerning the origin of spheroidal galaxies. The DEEP team thanks C. Steidel for sharing unpublished redshift data. The authors thank the Keck Observatory staff for their constant support during the several observing runs of DEEP1 and DEEP2; the W. M. Keck Foundation and NASA for construction of the Keck telescopes; and Bev Oke and Judy Cohen for their tireless work on LRIS that enabled the spectroscopic observations of DEEP1 galaxies. We also wish to recognize and acknowledge the highly significant cultural role and reverence that the summit of Mauna Kea has always had within the indigenous Hawaiian community; it is a privilege to be given the opportunity to conduct observations from this mountain.

The DEEP1 and DEEP2 surveys were founded under the auspices of the NSF Center for Particle Astrophysics. The bulk of the work was supported by National Science Foundation grants AST 95-29098 and 00-71198 to UCSC and AST 00-71048 to UCB. Additional support came from NASA grants AR-05801.01, AR-06402.01, and AR-07532.01 from the Space Telescope Science Institute, which is operated by AURA, Inc., under NASA contract NAS 5-26555. The DEIMOS spectrograph was funded

by NSF grant ARI92-14621 and by generous grants from the California Association for Research in Astronomy, and from UCO/Lick Observatory. HST imaging of the Groth Strip was planned, executed, and analyzed by Ed Groth and Jason Rhodes with support from NASA grants NAS5-1661 and NAG5-6279 from the WFPC1 IDT. SMF would like to thank the California Association for Research in Astronomy for a generous research grant and the Miller Institute at UC Berkeley for the support of a Visiting Miller Professorship. CW was supported by a PPARC fellowship. NPV acknowledges support from NASA grant GO-07883.01-96A and NSF grants NSF-0349155 from the Career Awards Program and NSF-0123690 via the ADVANCE Institutional Transformation Program at NMSU. KG was supported by Hubble Fellowship grant HF-01090.01-97A awarded by the Association of Universities for Research in Astronomy, Inc., for NASA under contract NAS5-26555. JAN acknowledges support from NASA through Hubble Fellowship grant HST-HF-01165.01-A awarded by the Space Telescope Science Institute, which is operated by the Association of Universities for Research in Astronomy, Inc., for NASA, under contract NAS 5-26555. Computer hardware gifts from Sun Microsystems and Quantum, Inc. are gratefully acknowledged. This research has made use of the NASA/IPAC Extragalactic Database (NED), which is operated by the Jet Propulsion Laboratory, California Institute of Technology, under contract with the National Aeronautics and Space Administration. Finally, we acknowledge NASA’s Astrophysics Data System Bibliographic Services.

REFERENCES

- Arp, H. A. 1966, *ApJS*, 14, 1
 Baade, D., et al. 1998, *The Messenger*, 93, 13
 Baade, D., et al. 1999, *The Messenger*, 95, 15
 Baade, W., & Gaposchkin, C. H. P. 1963, *Evolution of the Stars and Galaxies* (Cambridge: Harvard University Press)
 Baldry, I. K., Glazebrook, K., Brinkmann, J., Ivezić, Z., Lupton, R. H., Nichol, R. C., & Szalay, A. S. 2004, *ApJ*, 600, 681
 Balogh, M. L., Baldry, I. K., Nichol, R., Miller, C., Bower, R. G., & Glazebrook, K. 2004, *ApJ*, 615, 101
 Bardeen, J. M., Bond, J. R., Kaiser, N., & Szalay, A. S. 1986, *ApJ*, 304, 15
 Barnes, J., & Hernquist, L. 1996, *ApJ*, 471, 115
 Baugh, C. M., Cole, S., & Frenk, C. S. 1996, *MNRAS*, 283, 1361
 Bell, E. F., McIntosh, D. H., Katz, N., & Weinberg, M. D. 2003, *ApJS*, 149, 289
 Bell, E. F., et al. 2004a, *ApJ*, 600, 11L
 Bell, E. F., et al. 2004b, *ApJ*, 609, 752 (B04)
 Bender, R., Burstein, D., & Faber, S. M. 1992, *ApJ*, 399, 462
 Benson, A. J., Bower, R. G., Frenk, C. S., Lacey, C. G., Baugh, C. M., & Cole, S. 2003, *ApJ*, 599, 38
 Bernardi, M., Sheth, R. K., Nichol, R. C., Schneider, D. P., & Brinkmann, J. 2005, 129, 61
 Bernardi, M., et al. 1998, *ApJ*, 508, 143
 Bernardi, M., et al. 2003, *AJ*, 125, 1849
 Bertin, E., & Arnouts, S. 1996, *A&AS*, 117, 393
 Binggeli, B., Sandage, A., & Tammann, G. A. 1988, *ARAA*, 26, 509
 Binney, J., & Merrifield, M. 1998, *Galactic Astronomy* (Princeton: Princeton University Press)
 Blanton, M. R., et al. 2001, *AJ*, 121, 2358
 Blanton, M. R., et al. 2003, *ApJ*, 592, 819
 Blumenthal, G. R., Faber, S. M., Primack, J. R., & Rees, M. J. 1984, *Nature*, 311, 517
 Bolzonella, M., Pelló, R., & Maccagni, D. 2002, *A&A*, 395, 443
 Bower, R. G., Lucey, J. R., & Ellis, R. S. 1992, *MNRAS*, 254, 601
 Brinchmann, J., et al. 1998, *ApJ*, 499, 112
 Bromley, B. C., Press, W. H., Lin, H., & Kirshner, R. P. 1998, *ApJ*, 505, 25
 Bundy, K., Ellis, R. S., & Conselice, C. 2005, *astro-ph/0502204*
 Bundy, K., Fukugita, M., Ellis, R. S., Kodama, T., & Conselice, C. 2004, *ApJ*, 601, L123
 Cen, R., & Ostriker, J. P. 1993, *ApJ*, 417, 415
 Charlot, S., & Silk, J. 1994, *ApJ*, 432, 453
 Chen, H.-W. et al., 2003, *ApJ*, 586, 745
 Cimatti, A., et al. 2002a, *A&A*, 381, L68
 Cimatti, A., et al. 2002b, *A&A*, 392, 395
 Cimatti, A., et al. 2003, *A&A*, 412, L1
 Cimatti, A., et al. 2004, *Nature*, 430, 184
 Cohen, J. G. 2002, *ApJ*, 567, 672
 Coil, A. L., et al. 2004, *ApJ*, 609, 525
 Coleman, C. D., Wu, C.-C., & Weedman, D. W. 1980, *ApJS*, 43, 393
 Colless, M., Burstein, D., Davies, R. L., McMahon, R. K., Saglia, R. P., & Wegner, G. 1999, *MNRAS*, 303, 813

- Cooray, A., & Sheth, R. 2002, *Physics Reports*, 372, 1
- Cowie, L. L., Songaila, A., Hu, E. M., & Cohen, J. G. 1996, *AJ*, 112, 839
- Cox, T. J., Jonsson, P., Primack, J. R., & Somerville, R. S. 2004, astro-ph/0503201
- Cross, N. J., et al. 2004, *AJ*, 128, 1990
- Cuillandre, J.-C., Luppino, G., Starr, B., & Isani, S. 2001, in *Proceedings of Semaine de l'Astrophysique Française*, eds. F. Combes, D. Barret, F. Thévenin (Les Ulis: EdP-Sciences), 605
- Daddi, E., et al. 2005, astro-ph/0503102
- Davies, R. L., Efstathiou, G., Fall, S. M., Illingworth, G., & Schechter, P. L. 1983, *ApJ*, 266, 41
- Davis, M., & Huchra, J. P. 1982, *ApJ*, 254, 437
- Davis, M., et al. 2003, *SPIE*, 4834, 161
- de Lapparent, V., Arnouts, S., Galaz, G., & Bardelli, S. 2003, *A&A*, 404, 845
- de Lucia et al. 2004, *ApJ*, 610, L77
- de Vaucouleurs, G., 1977, in *Evolution of Galaxies and Stellar Populations*, eds. B. M. Tinsley & R. Larson (New Haven: Yale University Press), p. 43
- de Vaucouleurs, G., de Vaucouleurs, A., Corwin, H. G., Buta, R. J., Paturel, G., & Fouqué, P. 1991, *The Third Reference Catalog of Galaxies* (New York: Springer Verlag) (RC3)
- Dekel, A., & Birnboim, Y. 2004, astro-ph/0412300
- Djorgovski, S., & Davis, M. 1987, *ApJ*, 313, 59
- Dressler, A. 1980, *ApJ*, 236, 351
- Dressler, A., Faber, S. M., Burstein, D., Davies, R. L., Lynden-Bell, D., Terlevich, R. J., & Wegner, G. 1987, *ApJ*, 313, 37
- Drory, N., Bender, R., Feulner, G., Hopp, U., Maraston, C., Snigula, J., & Hill, G. J. 2003, *ApJ*, 595, 698
- Drory, N., Bender, R., Feulner, G., Hopp, U., Maraston, C., Snigula, J., & Hill, G. J. 2004, *ApJ*, 608, 742
- Drory, N., Salvato, M., Gabasch, A., Bender, R., Hopp, U., Feulner, G., & Pannella, M. 2005, *ApJ*, 619, L131
- Eales, S. 1993, *ApJ*, 404, 51
- Eggen, O. J., Lynden-Bell, D., & Sandage, A. R. 1962, *ApJ*, 136, 748
- Efstathiou, G., Ellis, R. S., & Peterson, B. A. 1988, *MNRAS*, 232, 441
- Faber, S. M. 1973, *ApJ*, 179, 731
- Faber, S. M., Dressler, A., Davies, R. L., Burstein, D., & Lynden-Bell, D. 1987, in *Nearly Normal Galaxies*, ed. S. M. Faber (New York: Springer Verlag), p. 175
- Faber, S. M., et al. 1997, *ApJ*, 114, 1771
- Faber, S. M., et al. 2003, *SPIE*, 4841, 1657
- Felten, J. E. 1976, *ApJ*, 207, 700
- Ferrarese, L., & Merritt, D. 2000, *ApJ*, 539, L9
- Fioc, M., & Rocca-Volmerange, B. 1997, *A&A*, 326, 950
- Förster Schreiber, N. M., et al. 2004, *ApJ*, 616, 40
- Folkes, S., et al. 1999, *MNRAS*, 308, 459
- Fontana, A., et al. 2004, *A&A*, 424, 23
- Franx, M., et al. 2003, *ApJ*, 587, L79
- Fried, J. W., et al. 2001, *A&A*, 367, 788
- Gabasch, A., et al. 2004, *A&A*, 421, 41 (FDF)
- Gebhardt, K., et al. 2000, *ApJ*, 543, L5
- Gebhardt, K. et al. 2003, *ApJ*, 597, 239
- Giallongo, E., et al. 2005, *ApJ*, 622, 116
- Gilbank, D. G., Smail, I., Ivison, R. J., & Packham, C. 2003, *MNRAS*, 346, 1125
- Gonzalez, J. J. 1993, PhD thesis, University of California, Santa Cruz
- Granato, G. L., de Zotti, G., Silva, L., Bressan, A., & Danese, L. 2004, *ApJ* 600, 580
- Groth, E. J., Kristian, J. A., Lynds, R., O'Neill, E. J., Balsano, R., Rhodes, J., & WFPC1 IDT 1994, *BAAS*, 26, 1403
- Häring, N., & Rix, H.-W. 2004, *ApJ*, 604, L89
- Hammer, F., Flores, H., Elbaz, D., Zheng, X. Z., Liang, Y. C., & Cesarsky, C. 2005, *A&A*, 430, 115
- Heavens, A., Panter, B., Jimenez, R. & Dunlop, J. 2004, *Nature*, 428, 625
- Heyl, J., Colless, M., Ellis, R. S., & Broadhurst, T. 1997, *MNRAS*, 285, 613
- Hibbard, J. E. 1995, PhD thesis, Columbia University
- Hogg, D. et al. 2002, *AJ*, 124, 646
- Hogg, D. et al. 2003, *ApJ*, 585, 5
- Ilbert, O., et al. 2004, astro-ph/0409134 (VVDS)
- Im, M., et al. 2001, *AJ*, 122, 720
- Im, M., et al. 2002, *ApJ*, 571, 1361
- Jonsson, P., Cox, T. J., Primack, J. R., & Somerville, R. S. 2005, astro-ph/0503135
- Jørgensen, I. 1999, *MNRAS*, 306, 607
- Juneau, S., et al. 2005, *ApJ*, 619, L135
- Kauffmann, G., Charlot, S., & White, S. D. M. 1996, *MNRAS*, 283, L117
- Kauffmann, G., et al. 2003a, *MNRAS*, 341, 33
- Kauffmann, G., et al. 2003b, *MNRAS*, 341, 54
- Kinney, A. L., Calzetti, D., Bohlin, R. C., McQuade, K., Storchi-Bergmann, T., & Schmitt, H. R. 1996, *ApJ*, 467, 38
- Kodama, T., Balogh, M. L., Smail, I., Bower, R. G., & Nakata, F. 2004, *MNRAS*, 354, 1103
- Kodama, T., et al. 2004, *MNRAS*, 350, 1005
- Koo, D. C., et al. 1996, *ApJ*, 469, 535
- Koo, D. C., et al. 2005, *ApJS*, 157, 175
- Kormendy, J., & Bender, R. 1996, *ApJ*, 464, L119
- Kormendy, J., & Richstone, D. 1995, *ARAA*, 33, 581
- Labbe, I., et al. 2005, astro-ph/0504219
- Larson, R. B. 1975, *MNRAS*, 173, 671
- Le Fèvre, O., Crampton, D., Hammer, F., Lilly, S. J., & Tresse, L. 1994, *ApJ* 423, L89
- Le Fèvre, O., Crampton, D., Lilly, S. J., Hammer, F. & Tresse, L. 1995, *ApJ*, 455, 60
- Le Fèvre, O., et al. 2004, astro-ph/0409123
- Lilly, S. J., Hammer, F., Le Fèvre, O., & Crampton, D. 1995a, *ApJ*, 455, 75
- Lilly, S. J., Le Fèvre, O., Hammer, F., & Crampton, D. 1996, *ApJ*, 460, L1
- Lilly, S. J., Tresse, L., Hammer, F., Crampton, D., & Le Fèvre, O. 1995b, *ApJ*, 455, 108
- Lilly, S. J., et al. 1998, *ApJ*, 500, 75
- Lin, H., et al. 1999, *ApJ*, 518, 533
- Lin, L., et al. 2004, *ApJ*, 617, L9
- Liske, J., Lemon, D. J., Driver, S. P., Cross, N. J., & Couch, W. J. 2003, *MNRAS*, 344, 307
- Longhetti, M., et al. 2005, astro-ph/0505467
- Loveday, J., Peterson, B. A., Efstathiou, G. P., & Maddox, S. J. 1992, *ApJ*, 390, 338
- Madgwick, D., et al. 2002, *MNRAS*, 333, 133
- Madgwick, D., et al. 2003, *ApJ*, 599, 997
- Magorrian, J., et al. 1998, *AJ*, 115, 2285
- Marinoni, C., Monaco, P., Giuricin, G., & Constantini, B. 1999, *ApJ*, 521, 50
- Marzke, R. O., & da Costa, L. N. 1997, *AJ*, 113, 185
- Marzke, R. O., da Costa, L. N., Pellegrini, P. S., Willmer, C. N. A., & Geller, M. J. 1998, *ApJ*, 503, 617

- Marzke, R. O., Huchra, J. P., & Geller, M. J. 1994, *ApJ*, 428, 43
- McIntosh, D. H., et al. 2004, *astro-ph/0411772*
- Menanteau, F., Ellis, R. S., Abraham, R. G., Barger, A. J., & Cowie, L. L. 1999, *MNRAS*, 309, 208
- Mihos, C. J., & Hernquist, L. 1994, *ApJ*, 427, 112
- Mihos, C. J., & Hernquist, L. 1996, *ApJ*, 471, 115
- Moore, B., Katz, N., Lake, G., Dressler, A., & Oemler, A., Jr. 1996, *Nature*, 379, 613
- Moustakas, L., et al., 2004, *ApJ*, 600, L131
- Murray, N., Quataert, E., & Thompson, T. A. 2005, *ApJ*, 618, 569
- Newman, J. A., & Davis, M. 2002, *ApJ*, 564, 567
- Norberg, P., et al. 2002, *MNRAS*, 336, 907
- Oke, J. B., et al. 1995, *PASP*, 107, 135
- Page, M. J., & Carrera, F. J. 2000, *MNRAS*, 311, 433
- Poli, F., Menci, N., Giallongo, E., Fontana, A., Cristiani, A., & D'Odorico, S. 2001, *ApJ*, 551, L45
- Postman, M., & Geller, M. J. 1984, *ApJ*, 281, 95
- Press, W.H., Flannery, B.P., Teukolsky, S.A., Vetterling, W.T. 1992, *Numerical Recipes*, (Cambridge: Cambridge Univ. Press), 2nd ed.
- Ratnatunga, K. U., Griffiths, R. E., & Ostrander, E. J. 1999, *AJ*, 118, 86
- Rhodes, J., Refregier, A., & Groth, E. J. 2000, *ApJ*, 536, 79
- Richstone, D., et al. 1998, *Nature*, 395, 14
- Roberts, M. 1969, *AJ*, 74, 859
- Rudnick, G., et al. 2003, *ApJ*, 599, 847
- Sandage, A. R., Binggeli, B., & Tammann, G. A. 1985, *AJ*, 90, 1759
- Sandage, A. R., Tammann, G. A., & Yahil, A. 1979, *ApJ*, 172, 253 (STY)
- Sandage, A. R., & Visvanathan, N. 1978, *ApJ*, 225, 742
- Sanders, D. B., & Mirabel, I. F. 1996, *ARAA*, 34, 749
- Saracco, P., et al. 2005, *MNRAS*, 357, L40
- Schade, D., et al. 1999, *ApJ*, 525, 31
- Schechter, P. L. 1976, *ApJ*, 203, 297
- Schmidt, M. 1968, *ApJ*, 151, 393
- Schweizer, F. 1982, *ApJ*, 252, 455
- Schweizer, F. 1986, *Science*, 231, 227
- Searle, L., Sargent, W. L. W., & Bagnuolo, W. G. 1973, *ApJ*, 179, 427
- Simard, L., et al. 1999, *ApJ*, 519, 563
- Simard, L., et al. 2002, *ApJS*, 142, 1
- Somerville, R. S., Lee, K., Ferguson, H. C., Gardner, J. P., Moustakas, L. A., & Giavalisco, M. 2004, 600, L171
- Springel, V., diMatteo, T., & Hernquist, L. 2005, *ApJ*, 620, L79
- Strateva, I., et al. 2001, *AJ*, 122, 1861
- Takeuchi, T. T., Yoshikawa, K., & Ishii, T. T. 2000, *ApJS*, 120, 1
- Tinsley, B. M. 1968, *ApJ*, 151, 547
- Toft, S., van Dokkum, P. G., Franx, M., Thompson, R. I., Illingworth, G. D., Bouwens, R. J., & Kriek, M. 2005, *ApJ*, 624, L9
- Toomre, A., & Toomre, J. 1972, *ApJ*, 178, 623
- Toomre, A., 1977, in *Evolution of Galaxies and Stellar Populations*, eds. B. M. Tinsley & R. Larson (New Haven: Yale University Press), p. 401
- Totani, T., & Yoshii, Y. 1998, *ApJ*, 501, L177
- Trager, S. C., Faber, S. M., Worthey, G., & Gonzalez, J. J. 2000a, *AJ*, 119, 1645
- Trager, S. C., Faber, S. M., Worthey, G., & Gonzalez, J. J. 2000b, *AJ*, 120, 165
- Tremaine, S., et al. 2002, *ApJ*, 574, 740
- Tremonti, C. A., et al. 2004, *ApJ*, 613, 898
- Tresse, L. 1999, *astro-ph/9902209*
- Treu, T., Ellis, R. S., Liao, T. X., & van Dokkum, P. 2005a, *ApJ*, 622, L5
- Treu, T., et al. 2005b, *astro-ph/0503164*
- Trujillo, I., & Aguerri, J. A. L. 2004, *MNRAS*, 355, 82
- Tyson, J. A., & Jarvis, J. F. 1979, *ApJ*, 230, 153
- van den Bergh, S. 1976, *ApJ*, 208, 17
- van der Wel, A., Franx, M., van Dokkum, P. G., Rix, H.-W., Illingworth, G. D., & Rosati, P. 2005, *astro-ph/05020228*
- van Dokkum, P. G., & Ellis, R. S. 2003, *ApJ*, 592, 53
- van Dokkum, P. G., & Franx, M. 2001, *ApJ*, 553, 90
- van Dokkum, P. G., Franx, M., Fabricant, D., Illingworth, G. D., & Kelson, D. D. 2000, *ApJ*, 541, 95
- van Dokkum, P. G., et al. 2003, *ApJ*, 587, L83
- van Dokkum, P. G., et al. 2004, *ApJ*, 611, 703
- Vogt, N. P., et al., 2005, *ApJS*, in press
- Weiner, B. J., et al., 2005, *ApJ*, 620, 595
- Willmer, C. N. A., et al. 2005, *ApJ*, submitted, *astro-ph/0506041*, (Paper I)
- Wolf, C., Meisenheimer, K., Rix, H.-W., Borch, A., Dye, S., & Kleinheinrich, M. 2003, *A&A*, 401, 73 (W03)
- Wolf, C., Meisenheimer, K., & Röser, H.-J. 2001, *A&A*, 365, 660
- Wolf, C., et al. 2004, *A&A*, 421, 913 (W04)
- Worthey, G., & Collobert, M. 2003, *ApJ*, 586, 17
- Worthey, G., Faber, S. M., & Gonzalez, J. J. 1992, *ApJ*, 398, 69
- Worthey, G., Trager, S. C., & Faber, S. M. 1995, in *Fresh Views of Elliptical Galaxies: ASP Conference Series*, Vol. 86, eds. A. Buzzoni, A. Renzini, and A. Serrano (San Francisco: Astronomical Society of the Pacific), p. 203
- Yan, L., & Thompson, D. 2003, *ApJ*, 586, 765

Figure f1 is available as file 0506044.f1.jpg

FIG. 1.— Apparent color-magnitude distribution of galaxies in the DEEP1 Groth Strip Survey. Panel *a* shows the full sample, panel *b* the distribution of galaxies placed on slits, and panel *c* the distribution of successful redshifts, where galaxies in the main DEEP1 redshift interval are shown as green triangles and galaxies lying beyond the upper redshift limit are shown as red diamonds. Galaxies with redshifts coming from Lilly et al. (1995a) and Brinchmann et al. (1998) are the black crosses. Panel *d* shows the distribution of failed redshifts. The limit $I814 = 23.5$ adopted for the luminosity function analysis is shown as the vertical dotted line, while the black dashed line represents the limit $(V606 + I814)/2 = 24$ actually used to select galaxies for observation. The dashed grey lines show the boundaries in color and magnitude used for the redshift histograms in Figure 6.

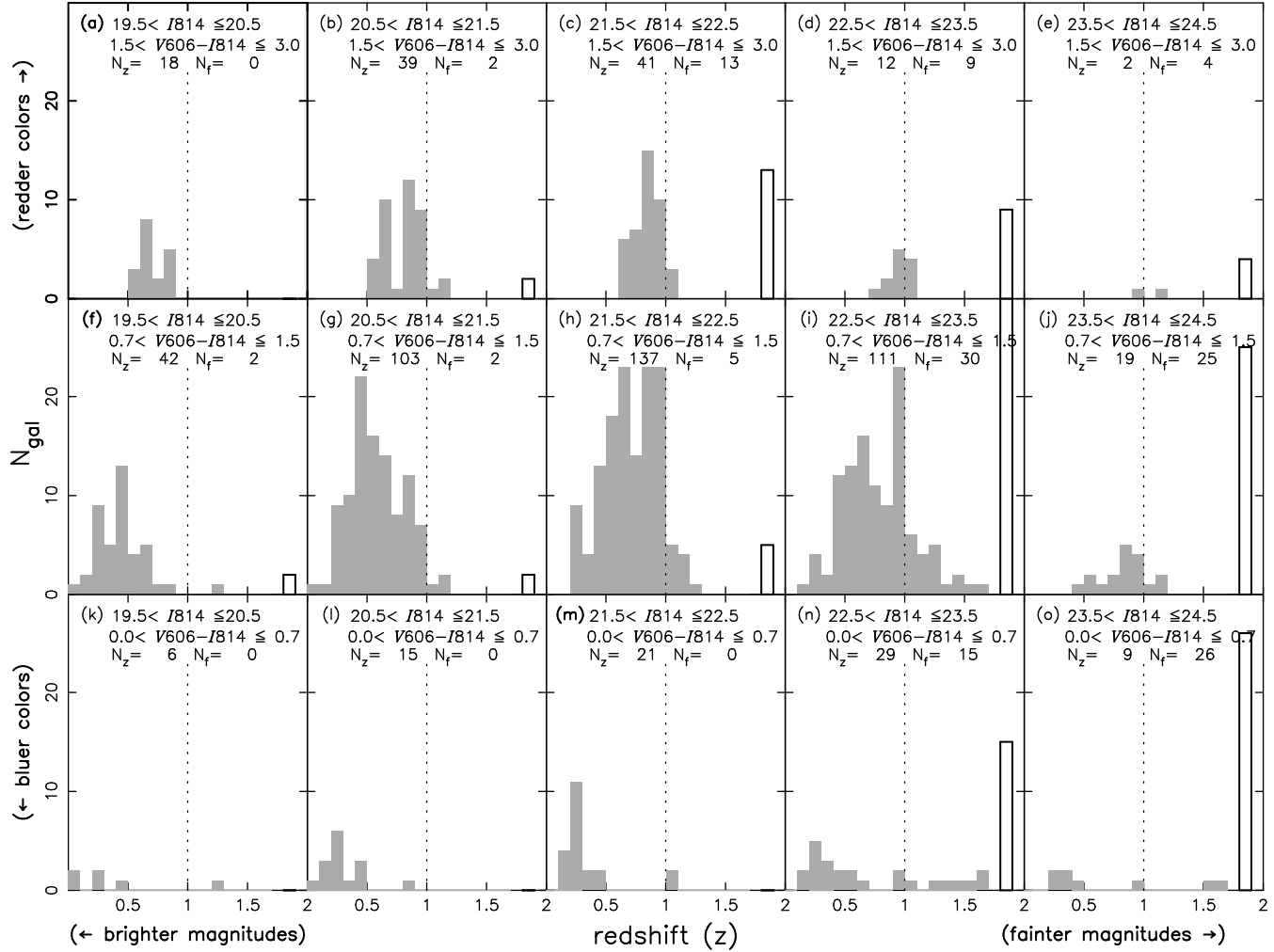


FIG. 2.— Distributions of measured DEEP1 redshifts in the apparent color-magnitude bins indicated in Figure 1. The display is such that magnitudes become fainter towards the right and colors redder towards the top. N_z in each panel is the number of successful redshifts in that bin; N_f is the number of attempted galaxies that failed to yield successful redshifts. The dashed line represents the high- z cut for DEEP1 ($z=1.0$), while the bar at the right of each diagram shows the number of failed redshifts. For $I814 \geq 22.5$, the number of failures increases significantly, being slightly larger for blue galaxies.

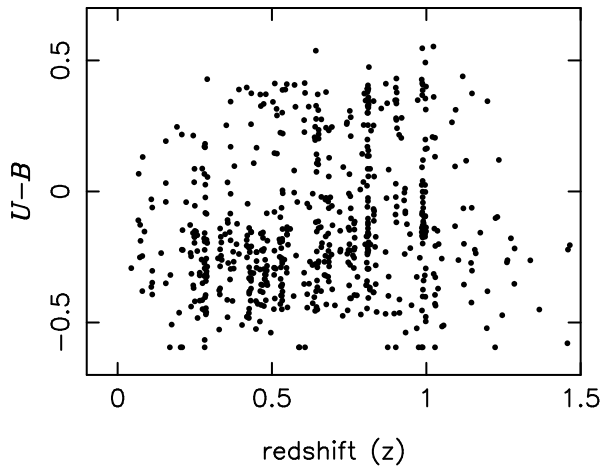


FIG. 3.— Rest-frame $(U - B)$ colors as a function of redshift for DEEP1 galaxies. The bimodal distribution of restframe colors is clearly evident. The lack of very low-redshift red galaxies is due to the small volume covered by DEEP1 and the rarity of faint red field galaxies.

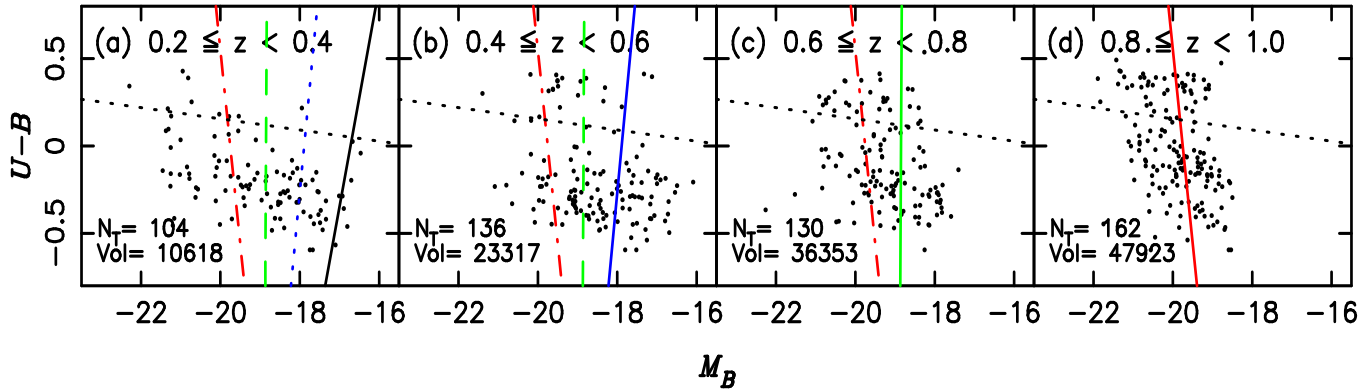


FIG. 4.— Rest-frame color-magnitude diagrams of DEEP1 galaxies for four redshift intervals. The solid line in each panel indicates the approximate faint absolute magnitude limit as a function of intrinsic color and redshift for a sample with a fixed apparent magnitude limit at $I_{814} = 23.5$. This line represents the faintest galaxy visible as a function of color at the upper redshift limit of each panel. The dashed lines repeat these solid lines from other panels. The dotted parallel line is the (fixed) cut used to define red-sequence galaxies, calculated in the same manner as for DEEP2 galaxies in Paper I. The numbers at lower left show the number of galaxies plotted and the co-moving volume in Mpc^3 for the $(H_0, \Omega, \Lambda) = (70, 0.3, 0.7)$ cosmology.

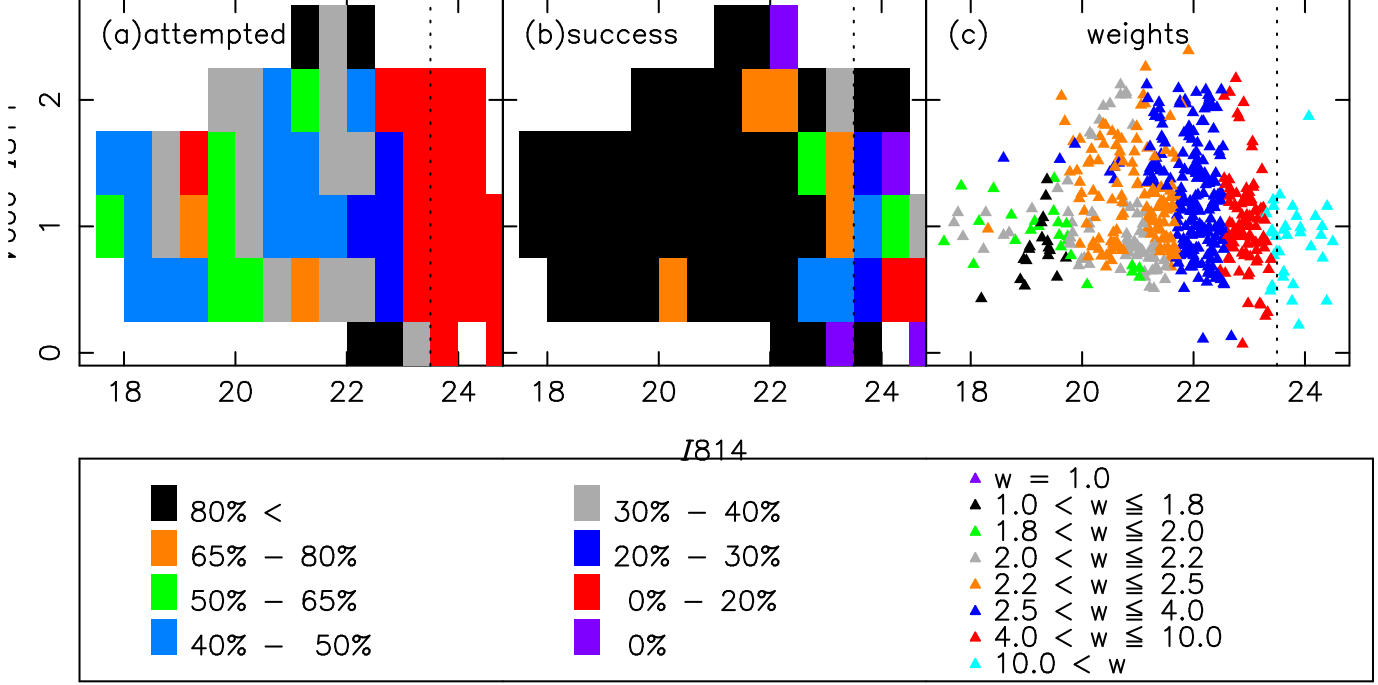


FIG. 5.— Sampling rate as a function of apparent magnitude and color for DEEP1. The vertical dotted line represents the $I_{814} = 23.5$ magnitude limit. Panel *a* shows the percentage of galaxies placed on slits relative to the total sample, panel *b* shows the success rate for obtaining good redshifts among those attempted, and panel *c* shows the weight of each galaxy used to correct for incomplete sampling as a function of color and apparent magnitude. The weighting scheme for all of DEEP1 uses the minimal model in which all failures correspond to galaxies beyond the upper redshift limit of the survey ($z > 1.0$).

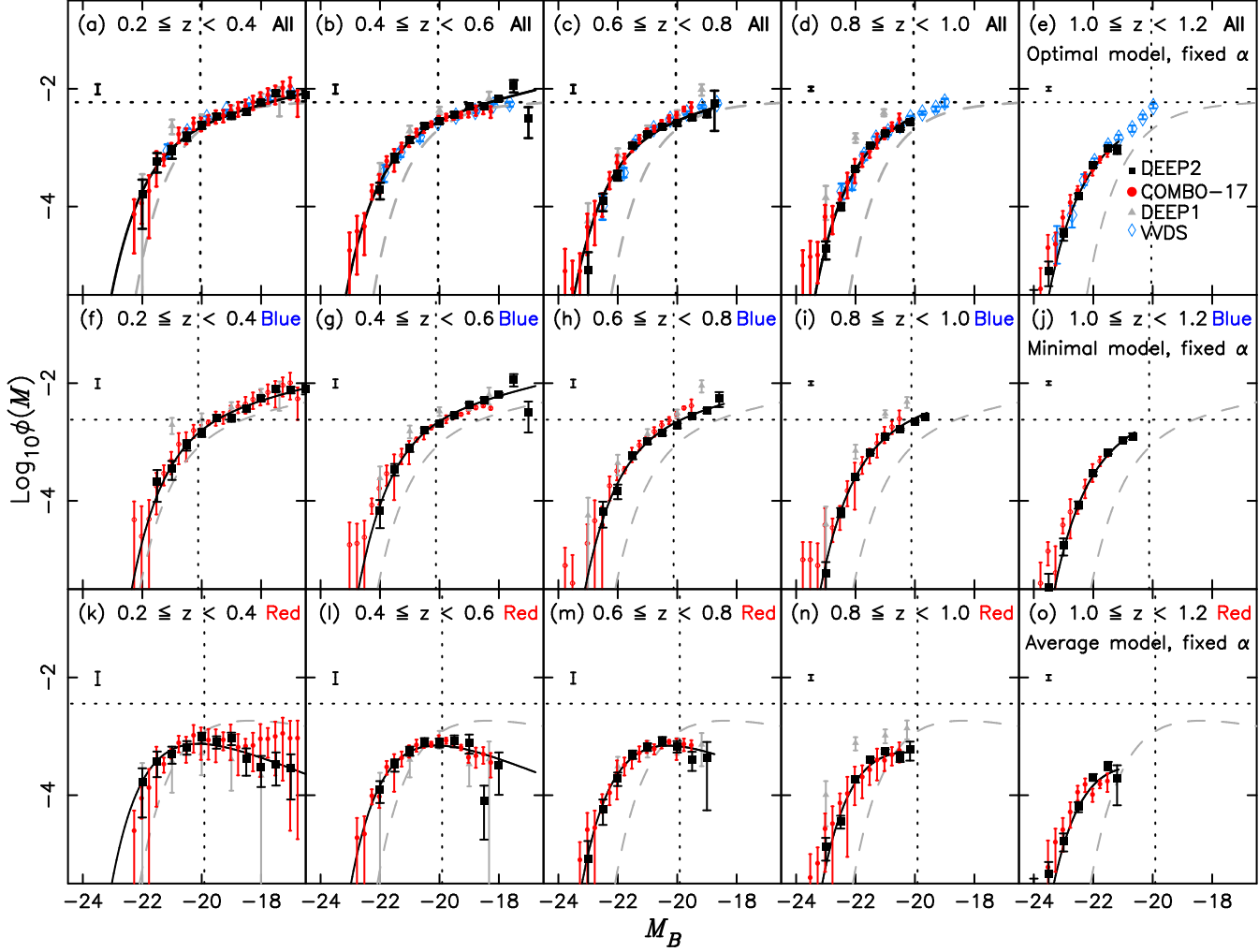


FIG. 6.— Luminosity functions measured in different redshift bins for “All” galaxies (top row), “Blue” galaxies (middle row), and “Red” galaxies (bottom row). Points determined using the $1/V_{max}$ method are shown as black squares for DEEP2, grey triangles for DEEP1, and red dots for COMBO-17. COMBO-17 data come from new calculations by C. Wolf using the revised bimodality method to separate blue and red galaxies. Similar points for All galaxies from VVDS (Ilbert et al. 2004) are shown as blue diamonds. Error bars for DEEP2 are 68% Poisson values only; those for COMBO-17 combine Poisson and cosmic variance. Cosmic variance for DEEP2 is shown at the top left of each panel based on theoretical values using the method described in the text; cosmic variance for COMBO-17 based on actual field-to-field measurements is similar (see Tables 2-4). The solid black lines represent Schechter functions fitted to DEEP2 data using the STY method. For these, α 's were kept fixed at the values measured from the COMBO-17 “quasi-local” sample in bins extending from $z = 0.2$ to 0.6. The values used are $\alpha = -1.3$ (All), $\alpha = -1.3$ (Blue), and $\alpha = -0.5$ (Red). Schechter functions for local samples are shown as the dashed grey lines, using results from SDSS measurements by Bell et al. (2003) as tabulated in Table 5. The dotted lines serve as a visual reference and are plotted at the values of M_B^* and ϕ^* for the local data. Overall the agreement between DEEP2, COMBO-17, and VVDS is very good where data overlap.

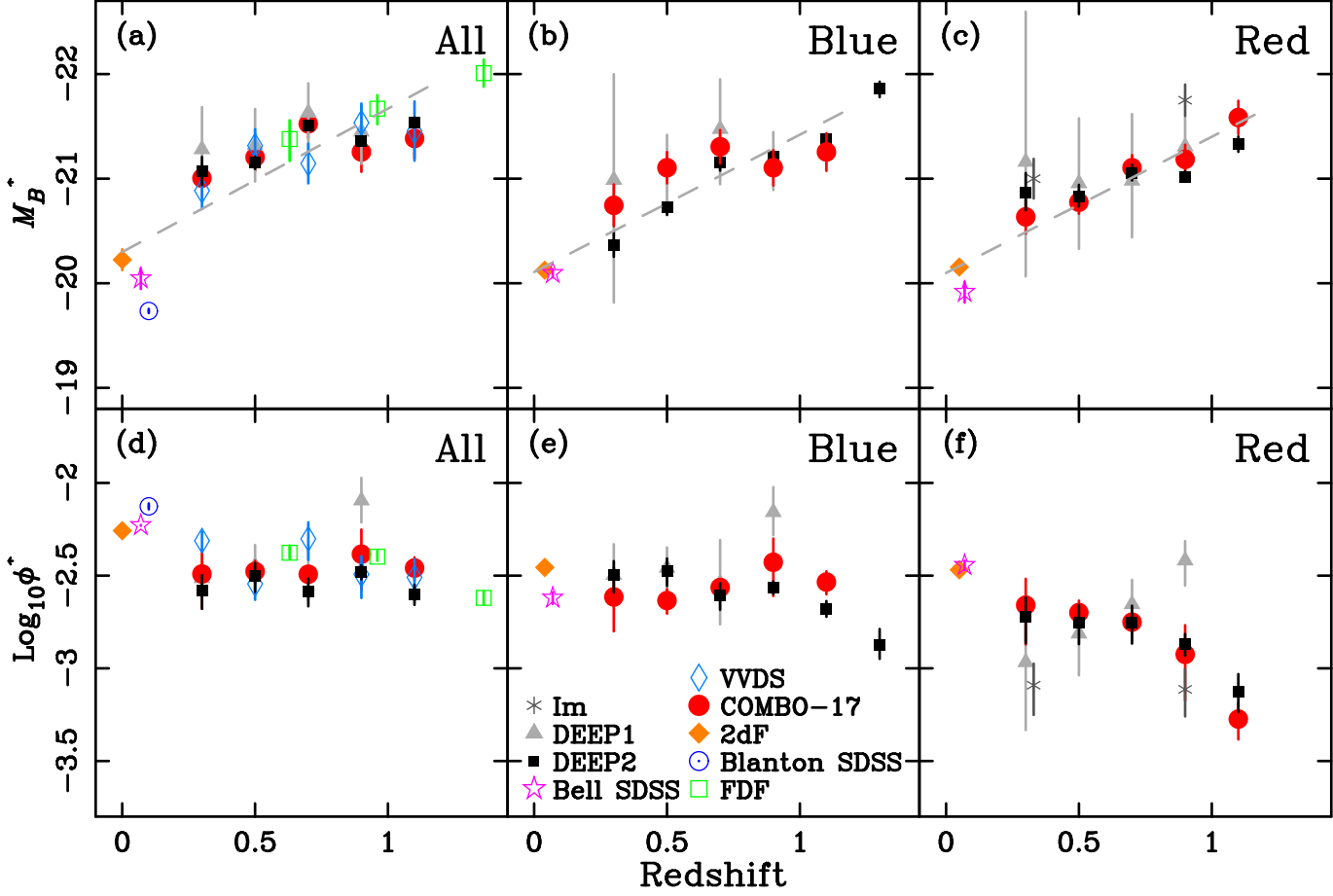


FIG. 7.— Evolution with redshift of the Schechter function parameters M_B^* (top panels) and ϕ^* (bottom panels) for the All, Blue and Red galaxy samples. Data values come from Tables 2-4. For DEEP2 and COMBO-17, these parameters were calculated keeping the faint-end slope parameter α fixed to the “quasi-local” COMBO-17 values (-1.3 [All], -1.3 [Blue] and -0.5 [Red]). Error bars on DEEP2 and COMBO-17 are Poisson 68% values for M_B^* and Poisson errors convolved in quadrature with cosmic variance for ϕ^* (see text). Also shown are the Schechter parameters from the other works summarized in Table 5. Estimates for distant galaxies come from Ilbert et al. (2004, VVDS, panels *a* and *d*) and Gabasch et al. (2004, FDF, panels *a* and *d*). Previous DEEP1 values from Im et al. (2002), are discussed in the text. Local values come from Bell et al. (2003) and Blanton et al. (2003) using SDSS and Norberg et al. (2002) and Madgwick et al. (2003) using 2dF. The trend of M_B^* becoming fainter towards lower redshifts is seen in all samples. The dashed grey lines represent linear fits to the evolution of M_B^* as a function of z , with coefficients shown in Table 6; M_B^* at $z \sim 1$ is ~ 1.3 magnitudes brighter than at $z = 0$ for all colors. Changes in galaxy number density (ϕ^*) vary with color; Blue number densities remain roughly constant to $z = 1$, Red number densities rise strongly with time, and the All sample is a blend of the two.

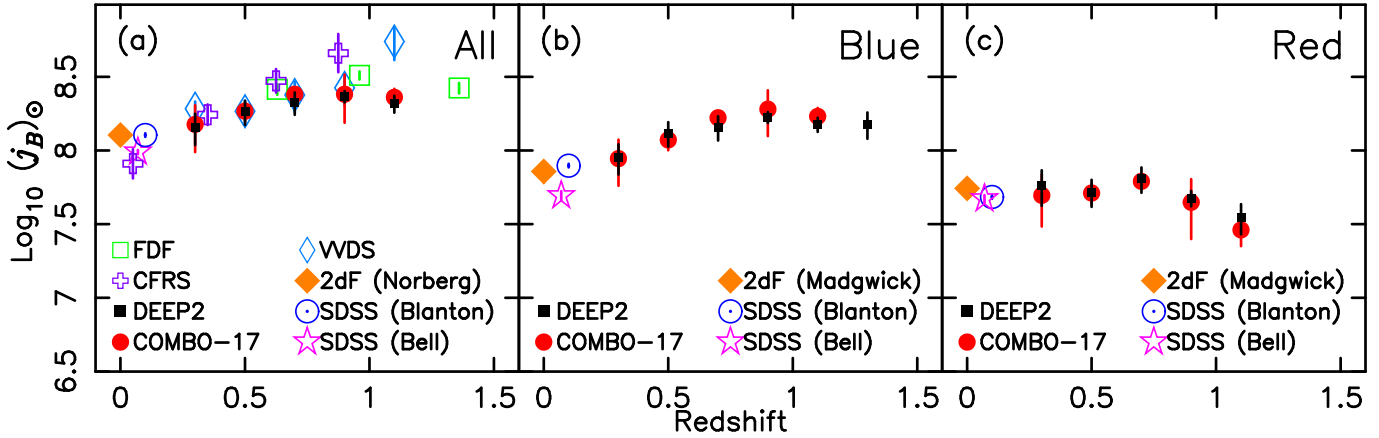


FIG. 8.— Evolution of the co-moving B -band luminosity density in units of solar luminosities per Mpc^{-3} , versus redshift. Data values come from Tables 2-4. References and symbols are the same as in Figure 7 except for CFRS (blue crosses), which comes from Lilly et al. (1996). The blue and red estimates from Blanton et al. (2003) use the total luminosity density from that paper, corrected by a contribution due to red galaxies of 38% from Hogg et al. (2003). The luminosity density of blue galaxies decreases with time by about a factor of 3 since $z = 1$, while that for red galaxies has remained roughly constant since $z = 0.9$, with a possible fall-off before that, in accordance with Bell et al. (2004a).

TABLE 1
SURVEY CHARACTERISTICS

| Survey | Area \square° | N_{field} | N_{gal} | N_z | $N_z > 0.8$ | m_l | m_u | z_{min} | z_{max} | System |
|--------------|-------------------------|-------------|-----------|-------|-------------|-------|-------|-----------|-----------|------------|
| (1) | (2) | (3) | (4) | (5) | (6) | (7) | (8) | (9) | (10) | (11) |
| EGS | 0.28 | 1 | 9115 | 4946 | 2026 | 18.5 | 24.1 | 0.2 | 1.4 | R_{AB} |
| Fields 2+3+4 | 0.85 | 3 | 18756 | 6338 | 4820 | 18.5 | 24.1 | 0.8 | 1.4 | R_{AB} |
| DEEP1 | 0.04 | 1 | 2438 | 621 | 241 | 16.5 | 23.5 | 0.2 | 1.0 | $I814Vega$ |
| COMBO 17 | 0.78 | 3 | 40210 | 27947 | 8792 | 17.0 | 24.0 | 0.2 | 1.2 | R_{Vega} |

Note. – The meanings of columns are: (1) surveyed region; (2) area in square degrees; (3) number of non-contiguous fields in surveyed region; (4) number of galaxies in source catalogue; (5) number of good quality redshifts; (6) number of good quality redshifts above $z = 0.8$; (7) bright apparent magnitude limit; (8) faint apparent magnitude limit; (9) lower redshift limit; (10) upper redshift limit; (11) apparent magnitude system of catalogue.

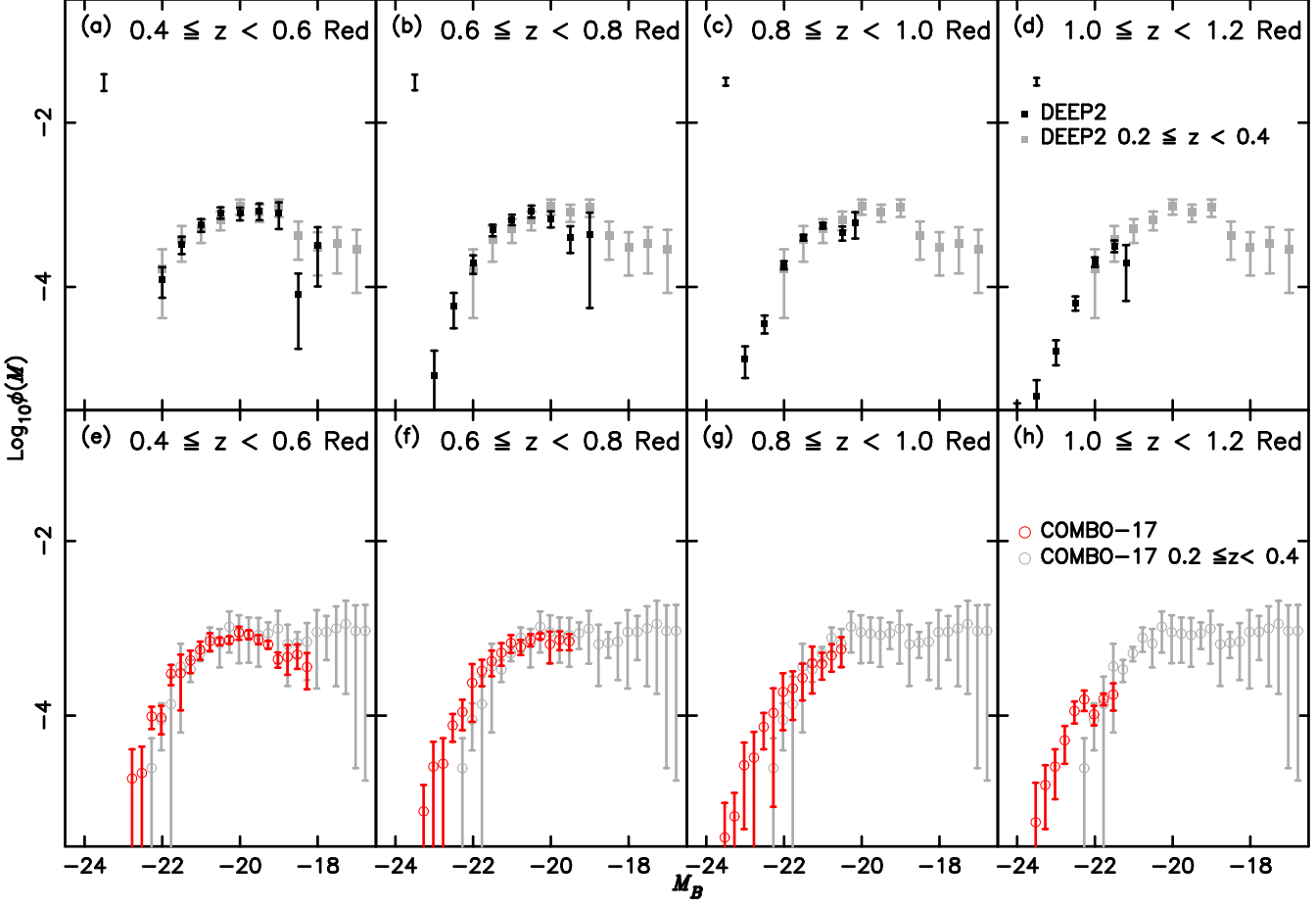


FIG. 9.— This figure overplots Red counts from the lowest-redshift bin (grey symbols) on top of counts at high redshift, for both DEEP2 and COMBO-17. The purpose is to illustrate how the Red counts do not evolve very much internally to each survey. The luminosity functions either stay fixed or translate parallel to themselves such that there is little change in numbers at constant absolute magnitude (over the magnitude range probed by the data). Both DEEP2 and COMBO-17 are the same in this regard. Fitted values of ϕ^* are decreasing and M_B^* are increasing throughout this range; though formally significant, these values clearly depend on subtle curvature in the data. However, stellar mass-to-light ratios are also increasing and, if taken into account, lead to the conclusion that the number density of galaxies *at fixed stellar mass* is falling approximately as ϕ^* .

The panels of this figure are available as files 0506044.f10.jpg, 0506044.f11.jpg and 0506044.f12.jpg

FIG. 10.— Schematic arrows showing galaxies migrating to the red sequence under different formation scenarios. Evolutionary tracks are plotted in the color-mass diagram. It is assumed that red galaxies arise from blue galaxies when star formation is quenched during a merger. This merger causes the galaxy to increase in mass (mass-doubling in equal-mass mergers is illustrated) while the stellar population reddens, as shown by the nearly vertical black arrows. These mergers would be gas-rich (or “wet”) because the merging galaxies are making stars and hence contain gas. Once a galaxy arrives on the red sequence, it may evolve further along it through a series of gas-poor, or “dry” mergers. These are shown as the white arrows. They are tilted upward to reflect the gradual aging of the stellar populations during dry merging. A major question in red-galaxy formation is the time of mass assembly versus the time of quenching. Three schematic possibilities are shown in the three panels. Track A represents very early quenching while the fragments of the galaxy are still small. In that case, most mass assembly occurs in dry mergers along the red sequence. Track B is extreme in the other sense, having maximally late quenching. In that case, galaxies assemble most of their mass while still blue and then merge once to become red, with no further dry merging. Track C is intermediate with a mixture of both histories. The properties of local E/S0 galaxies favor this “mixed” scenario.

TABLE 2
SCHECHTER FUNCTION PARAMETERS FOR ALL GALAXY SAMPLES

| $\langle z \rangle$ | N_{gal} | α | M_B^* | | ϕ^* | | \sqrt{Var} | j_B | Weights | | | |
|---------------------|-----------|----------|---------|-----------------|----------|-------------------|-----------------|-------|-----------------|-----------------------|---------|------|
| (1) | (2) | (3) | (4) | (5) | (6) | (7) | (8) | (9) | (10) | (11) | (12) | (13) |
| | | | | | | $\times 10^{-4}$ | Gal Mpc $^{-3}$ | | | $\times 10^8 L_\odot$ | | |
| 0.30 | 734 | -1.30 | -21.07 | (+ 0.13 - 0.13) | 26.39 | (+ 1.81 - 1.62) | | 0.20 | 1.43 \pm 0.33 | DEEP2 | optimal | |
| 0.50 | 983 | -1.30 | -21.15 | (+ 0.06 - 0.06) | 31.39 | (+ 0.97 - 1.04) | | 0.18 | 1.83 \pm 0.32 | DEEP2 | optimal | |
| 0.70 | 914 | -1.30 | -21.51 | (+ 0.03 - 0.03) | 26.07 | (+ 1.39 - 1.14) | | 0.16 | 2.11 \pm 0.34 | DEEP2 | optimal | |
| 0.90 | 2561 | -1.30 | -21.36 | (+ 0.01 - 0.02) | 33.04 | (+ 0.90 - 1.11) | | 0.08 | 2.33 \pm 0.20 | DEEP2 | optimal | |
| 1.10 | 844 | -1.30 | -21.54 | (+ 0.04 - 0.04) | 24.94 | (+ 2.20 - 2.63) | | 0.08 | 2.08 \pm 0.27 | DEEP2 | optimal | |
| 0.30 | 6205 | -1.30 | -21.00 | (+ 0.17 - 0.17) | 32.26 | (+ 11.32 - 11.32) | | 0.11 | 1.50 \pm 0.53 | COMBO-17 | | |
| 0.50 | 5828 | -1.30 | -21.20 | (+ 0.13 - 0.13) | 33.32 | (+ 4.73 - 4.73) | | 0.10 | 1.85 \pm 0.26 | COMBO-17 | | |
| 0.70 | 7122 | -1.30 | -21.52 | (+ 0.14 - 0.14) | 32.16 | (+ 2.91 - 2.91) | | 0.10 | 2.41 \pm 0.22 | COMBO-17 | | |
| 0.90 | 5795 | -1.30 | -21.25 | (+ 0.19 - 0.19) | 41.26 | (+ 14.84 - 14.84) | | 0.09 | 2.41 \pm 0.87 | COMBO-17 | | |
| 1.10 | 2997 | -1.30 | -21.38 | (+ 0.19 - 0.19) | 34.72 | (+ 4.97 - 4.97) | | 0.09 | 2.30 \pm 0.33 | COMBO-17 | | |

Note. – The meanings of columns are: (1) central redshift of bin; (2) number of galaxies in bin; (3) the value of the adopted faint-end slope; (4) the value of M_B^* , and upper (5) and lower (6) 68% Poisson errors; (7) mean density ϕ^* followed in columns (8) and (9) by the 68% Poisson errors for DEEP2 and combined Poisson with cosmic variance estimates for COMBO-17; (10) square root of cosmic variance, based on field geometry, bin volume and galaxy bias (b) as a function of color (see text) (11) luminosity density, followed in (12) by a conservative error that combines Poisson errors in M_B^* and ϕ^* with cosmic variance in quadrature; see text for further explanation (13) indicates the weighting scheme used. Optimal weights mean that minimal weights were used for blue galaxies and average weights were used for red galaxies. Both these and the COMBO-17 weights are explained in §3.

TABLE 3
SCHECHTER FUNCTION PARAMETERS FOR BLUE GALAXY SAMPLES

| $\langle z \rangle$ | N_{gal} | α | M_B^* | | ϕ^* | | \sqrt{Var} | j_B | Weights | | | |
|---------------------|-----------|----------|---------|-----------------|----------|-------------------|-----------------|-------|-----------------|-----------------------|---------|------|
| (1) | (2) | (3) | (4) | (5) | (6) | (7) | (8) | (9) | (10) | (11) | (12) | (13) |
| | | | | | | $\times 10^{-4}$ | Gal Mpc $^{-3}$ | | | $\times 10^8 L_\odot$ | | |
| 0.30 | 627 | -1.30 | -20.36 | (+ 0.13 - 0.11) | 31.78 | (+ 2.15 - 1.87) | | 0.11 | 0.89 \pm 0.20 | DEEP2 | minimal | |
| 0.50 | 812 | -1.30 | -20.72 | (+ 0.05 - 0.07) | 33.40 | (+ 1.39 - 1.77) | | 0.10 | 1.31 \pm 0.23 | DEEP2 | minimal | |
| 0.70 | 764 | -1.30 | -21.15 | (+ 0.07 - 0.07) | 24.67 | (+ 1.35 - 1.58) | | 0.09 | 1.44 \pm 0.26 | DEEP2 | minimal | |
| 0.90 | 2644 | -1.30 | -21.21 | (+ 0.00 - 0.03) | 27.27 | (+ 0.35 - 0.42) | | 0.09 | 1.68 \pm 0.13 | DEEP2 | minimal | |
| 1.10 | 1224 | -1.30 | -21.38 | (+ 0.04 - 0.05) | 20.84 | (+ 1.08 - 1.58) | | 0.09 | 1.50 \pm 0.16 | DEEP2 | minimal | |
| 1.30 | 448 | -1.30 | -21.86 | (+ 0.07 - 0.08) | 13.44 | (+ 2.00 - 2.71) | | 0.07 | 1.51 \pm 0.31 | DEEP2 | minimal | |
| 0.30 | 5109 | -1.30 | -20.74 | (+ 0.20 - 0.20) | 24.26 | (+ 8.42 - 8.42) | | 0.11 | 0.88 \pm 0.31 | COMBO-17 | | |
| 0.50 | 4649 | -1.30 | -21.10 | (+ 0.15 - 0.15) | 23.20 | (+ 3.48 - 3.48) | | 0.10 | 1.18 \pm 0.18 | COMBO-17 | | |
| 0.70 | 5691 | -1.30 | -21.30 | (+ 0.16 - 0.16) | 27.27 | (+ 3.12 - 3.12) | | 0.09 | 1.67 \pm 0.19 | COMBO-17 | | |
| 0.90 | 4903 | -1.30 | -21.10 | (+ 0.17 - 0.17) | 37.32 | (+ 12.80 - 12.80) | | 0.09 | 1.91 \pm 0.65 | COMBO-17 | | |
| 1.10 | 2741 | -1.30 | -21.25 | (+ 0.18 - 0.18) | 29.19 | (+ 4.14 - 4.14) | | 0.09 | 1.71 \pm 0.24 | COMBO-17 | | |

Note. – The meanings of columns are: (1) central redshift of bin; (2) number of galaxies in bin; (3) the value of the adopted faint-end slope; (4) the value of M_B^* , and upper (5) and lower (6) 68% Poisson errors; (7) mean density ϕ^* followed in columns (8) and (9) by the 68% Poisson errors for DEEP2 and combined Poisson with cosmic variance estimates for COMBO-17; (10) square root of cosmic variance, based on field geometry, bin volume and galaxy bias (b) as a function of color (see text) (11) luminosity density, followed in (12) by a conservative error that combines Poisson errors in M_B^* and ϕ^* with cosmic variance in quadrature; see text for further explanation (13) indicates the weighting scheme used. Minimal weights were used for blue galaxies and mean that all failed redshifts were assumed to lie beyond the upper limit of the survey, $z_h = 1.4$ for DEEP2. Both these and the COMBO-17 weights are explained further in §3.

TABLE 4
SCHECHTER FUNCTION PARAMETERS FOR RED GALAXY SAMPLES

| $\langle z \rangle$ | N_{gal} | α | M_B^* | | ϕ^* | | \sqrt{Var} | j_B | Weights | | | |
|---------------------|-----------|----------|---------|-----------------|----------|------------------|-----------------|-----------------|---------------|-----------------------|------|------|
| (1) | (2) | (3) | (4) | (5) | (6) | (7) | (8) | (9) | (10) | (11) | (12) | (13) |
| | | | | | | $\times 10^{-4}$ | Gal Mpc $^{-3}$ | | | $\times 10^8 L_\odot$ | | |
| 0.30 | 109 | -0.50 | -20.86 | (+ 0.16 - 0.17) | 18.89 | (+ 1.89 - 1.85) | 0.15 | 0.58 \pm 0.18 | DEEP2 average | | | |
| 0.50 | 173 | -0.50 | -20.83 | (+ 0.12 - 0.09) | 17.71 | (+ 1.03 - 1.13) | 0.14 | 0.52 \pm 0.13 | DEEP2 average | | | |
| 0.70 | 196 | -0.50 | -21.05 | (+ 0.06 - 0.06) | 17.63 | (+ 1.29 - 1.50) | 0.13 | 0.64 \pm 0.15 | DEEP2 average | | | |
| 0.90 | 535 | -0.50 | -21.02 | (+ 0.04 - 0.02) | 13.47 | (+ 0.60 - 0.82) | 0.12 | 0.47 \pm 0.06 | DEEP2 average | | | |
| 1.10 | 178 | -0.50 | -21.33 | (+ 0.08 - 0.07) | 7.51 | (+ 1.31 - 1.52) | 0.12 | 0.35 \pm 0.08 | DEEP2 average | | | |
| 0.30 | 1096 | -0.50 | -20.63 | (+ 0.16 - 0.16) | 21.91 | (+ 8.48 - 8.48) | 0.15 | 0.50 \pm 0.19 | COMBO-17 | | | |
| 0.50 | 1179 | -0.50 | -20.77 | (+ 0.11 - 0.11) | 19.97 | (+ 3.21 - 3.21) | 0.14 | 0.51 \pm 0.08 | COMBO-17 | | | |
| 0.70 | 1431 | -0.50 | -21.10 | (+ 0.12 - 0.12) | 17.75 | (+ 0.70 - 0.70) | 0.13 | 0.62 \pm 0.02 | COMBO-17 | | | |
| 0.90 | 892 | -0.50 | -21.18 | (+ 0.14 - 0.14) | 11.89 | (+ 5.20 - 5.20) | 0.12 | 0.45 \pm 0.19 | COMBO-17 | | | |
| 1.10 | 256 | -0.50 | -21.58 | (+ 0.16 - 0.16) | 5.32 | (+ 1.19 - 1.19) | 0.12 | 0.29 \pm 0.07 | COMBO-17 | | | |

Note. – The meanings of columns are: (1) central redshift of bin; (2) number of galaxies in bin; (3) the value of the adopted faint-end slope; (4) the value of M_B^* , and upper (5) and lower (6) 68% Poisson errors; (7) mean density ϕ^* followed in columns (8) and (9) by the 68% Poisson errors for DEEP2 and combined Poisson with cosmic variance estimates for COMBO-17; (10) square root of cosmic variance, based on field geometry, bin volume and galaxy bias (b) as a function of color (see text) (11) luminosity density, followed in (12) by a conservative error that combines Poisson errors in M_B^* and ϕ^* with cosmic variance in quadrature; see text for further explanation (13) indicates the weighting scheme used. Average weights were used for red galaxies and mean that all failed redshifts were assumed to follow the same redshift distribution as successfully observed galaxies. Both these and the COMBO-17 weights are explained further in §3.

TABLE 5
SCHECHTER FUNCTION PARAMETERS FROM THE LITERATURE

| Sample | z_{med} | α | M_B^* | | ϕ^* | | j_B | Reference | Notes | | |
|--------|-----------|------------------|---------|---------------|----------|------------------|-----------------|-----------------------|-------|------|------|
| (1) | (2) | (3) | (4) | (5) | (6) | (7) | (8) | (9) | (10) | (11) | (12) |
| | | | | | | $\times 10^{-4}$ | Gal Mpc $^{-3}$ | $\times 10^8 L_\odot$ | | | |
| A | 0.07 | -1.21 \pm 0.03 | -20.22 | (+0.10 -0.10) | 55.22 | (+ 4.46 -4.46) | 1.27 \pm 0.12 | 1 | a | | |
| A | 0.07 | -1.03 \pm 0.10 | -20.04 | (+0.10 -0.10) | 59.00 | (+ 0.34 - 0.34) | 0.98 \pm 0.03 | 2 | b | | |
| A | 0.10 | -0.89 \pm 0.01 | -19.73 | (+0.02 -0.02) | 74.77 | (+ 2.74 - 2.74) | 1.27 \pm 0.04 | 3 | | | |
| A | 0.30 | -1.16 \pm 0.03 | -20.88 | (+0.18 -0.18) | 48.74 | (+ 5.87 - 5.87) | 1.92 \pm 0.23 | 4 | c | | |
| A | 0.50 | -1.26 \pm 0.05 | -21.31 | (+0.16 -0.16) | 28.54 | (+ 5.14 - 5.14) | 1.85 \pm 0.33 | 4 | c | | |
| A | 0.70 | -1.10 \pm 0.11 | -21.14 | (+0.19 -0.19) | 49.87 | (+11.46 -11.46) | 2.38 \pm 0.55 | 4 | c | | |
| A | 0.90 | -1.30 \pm 0.11 | -21.53 | (+0.18 -0.18) | 32.10 | (+ 8.16 - 8.16) | 2.66 \pm 0.68 | 4 | c | | |
| A | 1.10 | -1.70 \pm 0.17 | -21.45 | (+0.28 -0.28) | 30.94 | (+ 7.85 - 7.85) | 5.50 \pm 1.40 | 4 | c | | |
| A | 0.63 | -1.25 \pm 0.17 | -21.38 | (+0.21 -0.18) | 42.00 | (+ 4.00 - 3.00) | 2.60 \pm 0.22 | 5 | | | |
| A | 0.96 | -1.25 \pm 0.17 | -21.67 | (+0.15 -0.13) | 40.00 | (+ 3.00 - 2.00) | 3.24 \pm 0.20 | 5 | | | |
| A | 1.36 | -1.25 \pm 0.17 | -22.01 | (+0.13 -0.13) | 24.00 | (+ 2.00 - 2.00) | 2.66 \pm 0.22 | 5 | | | |
| B | 0.04 | -1.24 \pm 0.01 | -20.12 | (+0.05 -0.05) | 34.99 | (+ 0.69 - 0.69) | 0.72 \pm 0.12 | 6 | a | | |
| B | 0.07 | -1.24 \pm 0.10 | -20.09 | (+0.04 -0.04) | 23.96 | (+ 1.73 - 1.73) | 0.49 \pm 0.04 | 2 | d | | |
| R | 0.04 | -0.54 \pm 0.02 | -20.15 | (+0.05 -0.05) | 33.96 | (+ 1.72 - 1.72) | 0.55 \pm 0.04 | 6 | a | | |
| R | 0.07 | -0.76 \pm 0.10 | -19.91 | (+0.10 -0.10) | 35.96 | (+ 2.06 - 2.06) | 0.47 \pm 0.03 | 2 | e | | |
| R | 0.33 | -1.00 | -21.00 | (+0.19 -0.19) | 7.10 | (+ 2.20 - 2.20) | ... | 7 | f | | |
| R | 0.90 | -1.00 | -21.75 | (+0.15 -0.15) | 6.80 | (+ 1.90 - 1.90) | ... | 7 | f | | |

The meanings of the columns are: (1) Sample : All galaxies (A), Blue (B) or Red (R); (2) median redshift of sample; (3) Schechter function faint-end slope and error; (4), (5) and (6) characteristic luminosity and errors ; (7), (8) and (9) Schechter function normalization and errors; (10) luminosity density and error; (11) reference; (12) additional notes. All quantities are converted to the $(H_0, \Omega_M, \Omega_\Lambda)$ cosmology of this paper and are calculated for $B_{Johnson}$ using the transformations listed in the individual footnotes. Those involving SDSS magnitudes and colors come from B04, using average colors $(g-r) = (0.82, 0.69, 1.01)$ for (All, Blue, Red) galaxies respectively.

References: (1) Norberg et al. 2002 ; (2) Bell et al. 2003; (3) Blanton et al. 2003.; (4) Ilbert et al. 2004; (5) Gabasch et al. 2004 ; (6) Madgwick et al. 2002; (7) Im et al. 2002.

^a $B_{Johnson} = b_j + 0.21$.

^b $B_{Johnson} = g + 0.115 + 0.370 \times 0.82$.

^c ϕ^* inferred from fits to VVDS data points fixing α and M_B^* .

^d $B_{Johnson} = g + 0.115 + 0.370 \times 0.69$.

^e $B_{Johnson} = g + 0.115 + 0.370 \times 1.01$.

^f Fixed α .

TABLE 6. EVOLUTION OF M^* FROM SDSS, 2dF, COMBO-17 AND DEEP2

| sample | $M^*(z-0.6)$ | | Q | |
|--------|--------------|------|------|------|
| All | -21.42 | 0.08 | 1.37 | 0.31 |
| Blue | -20.89 | 0.05 | 1.31 | 0.14 |
| Red | -20.87 | 0.05 | 1.30 | 0.20 |

NOTE. — The equation fitted is $M^*(z-0.6) = M^*(z-0.6) + Q(z-0.6)$. The fits are obtained weighting each value of M^* by its error, δM^* . The midpoint of the z -range was chosen as the horizontal zero-point to minimize correlated errors between M^* and Q .

This figure "f1.jpg" is available in "jpg" format from:

<http://arXiv.org/ps/astro-ph/0506044v3>

This figure "f10.jpg" is available in "jpg" format from:

<http://arXiv.org/ps/astro-ph/0506044v3>

This figure "f11.jpg" is available in "jpg" format from:

<http://arXiv.org/ps/astro-ph/0506044v3>

This figure "f12.jpg" is available in "jpg" format from:

<http://arXiv.org/ps/astro-ph/0506044v3>